Article

Fat1 deletion promotes hybrid EMT state, tumour stemness and metastasis

https://doi.org/10.1038/s41586-020-03046-1

Received: 21 January 2019

Accepted: 26 October 2020

Published online: 16 December 2020

Check for updates

Ievgenia Pastushenko[1,2,3,31], Federico Mauri[1,31], Yura Song[1], Florian de Cock[1], Bob Meeusen[4,5], Benjamin Swedlund[1], Francis Impens[6,7,8], Delphi Van Haver[6,7,8], Matthieu Opitz[9], Manuel Thery[10,11], Yacine Bareche[12], Gaelle Lapouge[1], Marjorie Vermeersch[13], Yves-Rémi Van Eycke[14,15], Cédric Balsat[14], Christine Decaestecker[14,15], Youri Sokolow[16], Sergio Hassid[17], Alicia Perez-Bustillo[18], Beatriz Agreda-Moreno[19], Luis Rios-Buceta[20,21,22], Pedro Jaen[20,21,22], Pedro Redondo[23], Ramon Sieira-Gil[24], Jose F. Millan-Cayetano[25], Onofre Sanmatrtin[26], Nicky D'Haene[27], Virginie Moers[1], Milena Rozzi[1], Jeremy Blondeau[1], Sophie Lemaire[1], Samuel Scozzaro[1], Veerle Janssens[4,5], Magdalena De Troya[25], Christine Dubois[1], David Pérez-Morga[13,28], Isabelle Salmon[27], Christos Sotiriou[12], Francoise Helmbacher[29] & Cédric Blanpain[1,30] ✉

FAT1, which encodes a protocadherin, is one of the most frequently mutated genes in human cancers[1–5]. However, the role and the molecular mechanisms by which *FAT1* mutations control tumour initiation and progression are poorly understood. Here, using mouse models of skin squamous cell carcinoma and lung tumours, we found that deletion of *Fat1* accelerates tumour initiation and malignant progression and promotes a hybrid epithelial-to-mesenchymal transition (EMT) phenotype. We also found this hybrid EMT state in *FAT1*-mutated human squamous cell carcinomas. Skin squamous cell carcinomas in which *Fat1* was deleted presented increased tumour stemness and spontaneous metastasis. We performed transcriptional and chromatin profiling combined with proteomic analyses and mechanistic studies, which revealed that loss of function of *FAT1* activates a CAMK2–CD44–SRC axis that promotes YAP1 nuclear translocation and *ZEB1* expression that stimulates the mesenchymal state. This loss of function also inactivates EZH2, promoting *SOX2* expression, which sustains the epithelial state. Our comprehensive analysis identified drug resistance and vulnerabilities in *FAT1*-deficient tumours, which have important implications for cancer therapy. Our studies reveal that, in mouse and human squamous cell carcinoma, loss of function of *FAT1* promotes tumour initiation, progression, invasiveness, stemness and metastasis through the induction of a hybrid EMT state.

FAT1 is very frequently mutated in a broad range of human cancers—in particular, in squamous cell carcinomas (SCCs)[1–5]. Mutations in *FAT1* have previously been associated with poor clinical outcome and resistance to anti-cancer therapy[6]. In skin SCCs induced by the chemical carcinogen 7,12-dimethylbenz[a]-anthracene (DMBA) in combination with 12-*O*-tetradecanoylphorbol-13-acetate (TPA) (hereafter, DMBA/TPA), *Fat1* is mutated in about 20% of cases[7], as in human SCCs. Stop–gain mutations are very frequently found, which indicates that these mutations result in loss of function (LOF) and that *FAT1* acts as a tumour-suppressor gene[1,4,8]. Knockdown of *FAT1* using short hairpin RNA in human cancer cell lines has previously been shown to decrease cell–cell adhesion and promote cell migration, whereas contradictory results have been obtained regarding the role of *FAT1* in regulating EMT in vitro[9,10]. However, a formal in vivo demonstration by a genetic LOF experiment that shows that *Fat1* acts as a tumour-suppressor gene is lacking. More importantly, the molecular mechanisms by which mutations in *FAT1* promote tumorigenesis and control tumour heterogeneity in vivo are completely unknown.

Fat1 deletion promotes malignant progression

To assess whether *Fat1* LOF promotes tumour initiation, we performed conditional deletion of *Fat1* in the skin epidermis using the constitutive *Krt14-cre* (*Krt14-cre;Fat1*$^{flox/flox}$*;Rosa26*$^{YFP/+}$; hereafter referred to as *Fat1*-constitutive knockout (*Fat1*-cKO)) mouse model. *Fat1*-cKO mice were born at a Mendelian ratio and did not present skin abnormalities (Extended Data Fig. 1). Following administration of DMBA/TPA, tumorigenesis developed more rapidly: the number of benign and malignant tumours per mouse was increased in *Fat1*-cKO mice, which demonstrates that *Fat1* acts a tumour-suppressor gene in DMBA/TPA-induced skin SCCs (Extended Data Fig. 2a–f). To assess the role of FAT1 in regulating malignant progression, we performed acute deletion of *Fat1* in benign papillomas using inducible *Krt14-creER* (*Krt14-creER;Fat1*$^{flox/flox}$*;Rosa26*$^{YFP/+}$). Immunostaining and electron microscopy analyses revealed that after deletion of *Fat1*, the polarity of the basal cells as well as the adherens and tight junctions were rapidly lost, the basal

A list of affiliations appears at the end of the paper.

lamina became discontinued, the hemidesmosomes were decreased and KRT10 expression—characteristic of benign tumour differentiation—was rapidly lost (Extended Data Fig. 2j–r).

These data demonstrate that *Fat1* deletion promotes malignant progression by controlling cell polarity and adhesion between tumour cells, and between tumour cells and the extracellular matrix.

Fat1 deletion promotes a hybrid EMT

The histological differences we observed in benign papillomas persisted in malignant SCCs. *Fat1*-cKO tumour cells were less cohesive and had rounded shapes; most of these tumour cells expressed the mesenchymal marker vimentin, which suggest that they underwent EMT. Fluorescence-activated cell sorting (FACS) analysis showed that *Fat1*-cKO SCCs contained a large proportion of EPCAM$^-$ cells, which was very rare in DMBA/TPA-induced SCCs with wild-type *Fat1*. The EMT occurred very early during tumour progression, as EPCAM$^-$ tumour cells could be detected in papillomas (Fig. 1a–c, Extended Data Fig. 3).

Distinct tumour EMT states—which are characterized by the expression of different levels of the cell-surface markers EPCAM, CD106, CD61 and CD51, and represent different stages within the EMT process—have recently been recognized[11]. The majority of the *Fat1*-cKO EPCAM$^-$ EMT tumour cells were negative for the CD106, CD61 and CD51 markers or expressed CD106 alone; these represent two hybrid EMT subpopulations characterized by the co-expression of epithelial and mesenchymal markers in genetically induced skin SCCs[11]. We performed cytospin on FACS-isolated tumour cells, which confirmed that *Fat1* deletion promoted the appearance of hybrid EMT subpopulations that co-express epithelial (KRT14) and mesenchymal (vimentin) markers (Fig. 1c–f). These data demonstrate that a genetic mutation in a tumour-suppressor gene can promote the acquisition of a hybrid EMT phenotype.

To assess whether *Fat1* LOF promotes the acquisition of a hybrid EMT phenotype in other models, we combined deletion of *Fat1* and *p53* (also known as *Trp53*) with *Kras*^{G12D} expression in different epidermal lineages. *Krt14-creER*, which targets the interfollicular epidermis, induces SCCs with well-differentiated phenotypes without EMT features, whereas *Lgr5-creER*—which targets the hair follicle—induces heterogeneous tumours characterized by different degrees of EMT[12]. Similar to what we found in DMBA/TPA-derived SCCs, loss of *Fat1* in the *Krt14-creER;Kras*^{G12D}*;p53*^{cKO}*;Fat1*^{cKO}*;Rosa26*$^{YFP/+}$ mouse model promoted the acquisition of a hybrid EMT phenotype, whereas *Lgr5-creER*-induced SCCs—which presented high proportion of EMT phenotypes independently of *Fat1* deletion—did not further increase EMT features upon *Fat1* LOF. By contrast with the control condition[11], most *Lgr5-creER Fat1*-cKO tumour cells continued to express KRT14 and presented signs of squamous differentiation that were visible as keratin pearls (Extended Data Fig. 4a–m). These data demonstrate that, in three independent mouse models of skin SCC, *Fat1* deletion promotes the acquisition of stable hybrid EMT phenotypes.

To assess whether the promotion of the tumour hybrid state by *Fat1* deletion is skin-specific or whether it is conserved across different types of tumour, we combined *Fat1* and *p53* deletion with *Kras*^{G12D} expression in the lung epithelia by intratracheal instillation of *cre*-expressing adenovirus. *Fat1* deletion considerably increased the number of tumours per lung (Extended Data Fig. 4n, o), and these tumours also presented signs of hybrid EMT. Whereas *Kras*^{G12D} expression and *p53* deletion promoted the onset of adenocarcinomas characterized by expression of NKX2-1 (also known as TTF1), the simultaneous deletion of *Fat1* promoted the formation of lung SCCs, which were characterized by a decreased expression of NKX2-1 as well as by SOX2 expression (Fig. 1g–l). This is consistent with the higher proportion of *FAT1* mutations found in lung SCCs relative other types of lung cancer[1,2], and suggests that *FAT1* mutations could be a driving force for the squamous tumour phenotype.

To assess the human relevance of our findings, we performed *FAT1* deletion using CRISPR–Cas9 in the A388 human epithelial SCC cell line, which contains wild-type *FAT1*. Upon *FAT1* deletion, cells were less cohesive and more rounded, had decreased expression of E-cadherin and co-expressed epithelial (KRT14, p63 and SOX2) and mesenchymal (vimentin and ZEB1) markers (Fig. 1m), which is reminiscent of the EMT hybrid state found in mouse SCCs. By sequencing patient-derived xenotransplants of SCCs from different organs, we identified SCCs with and without *FAT1* LOF mutations. Co-immunostaining of pan-cytokeratin and vimentin showed that *FAT1*-mutated SCCs exhibit a much higher EMT hybrid score as compared to SCCs with wild-type *FAT1* (Fig. 1n, o, Extended Data Fig. 5). These data show that *FAT1* mutations promote the acquisition of a hybrid EMT state in human cancers.

FAT1 deletion promotes stemness and metastasis

EMT has previously been associated with an increase in tumour stemness[11–14]. Tumour transplantation assays of *Fat1*-cKO and wild-type EPCAM$^+$ and EPCAM$^-$ tumour cells showed that *Fat1* LOF was associated with a tenfold increase in tumour-propagating cells as compared to *Fat1* wild type. The histology of the secondary tumours recapitulated the histology of the primary tumours (Fig. 2a, b). Tumour stemness is also associated with increased clonogenicity in vitro. To validate our findings, we assessed the clonogenicity of wild-type and *FAT1*-knockout human SCC cell lines in 3D tumour spheroid assays. *FAT1*-knockout cell lines grew much better than the isogenic wild-type control cell line (Fig. 2c, d). Altogether, these data show that *FAT1* deletion promotes tumour stemness in mouse and human cancers.

The hybrid EMT tumour state has previously been associated with the presence of circulating tumour cells and with increased metastatic potential upon intravenous injection of tumour cells[11]. Notably, the proportion of the mice presenting lymph node and lung metastases and the number of metastases per mouse were increased in *Fat1*-cKO mice (Fig. 2e–h). Intravenous injection of EPCAM$^+$ *Fat1*-cKO tumour cells gave rise to a higher number of lung metastasis as compared to tumour cells with wild-type *Fat1* (Fig. 2i–l), which demonstrates that *Fat1* LOF greatly increases spontaneous metastasis and lung colonization in skin SCCs, independently of the number of primary tumours or the occurrence of EMT. These data demonstrate that *Fat1*-LOF-induced hybrid EMT state promotes metastasis in vivo.

Gene signature of *Fat1*-mutated tumours

To investigate the molecular mechanisms by which *Fat1* LOF promotes the hybrid EMT state, we first assessed the transcriptional signature of *Fat1*-mutated tumour cells from mouse skin SCCs. RNA sequencing (RNA-seq) revealed that *Fat1*-cKO EPCAM$^+$ tumour cells presented a strong upregulation of many well-known EMT markers—including *Vim*, *Snai1*, *Prrx1*, *Twist1*, *Zeb1* or *Zeb2*—and the expression of these genes was further upregulated in EPCAM$^-$ *Fat1*-knockout tumour cells, which suggests that EPCAM$^+$ *Fat1*-cKO tumour cells are transcriptionally primed to undergo EMT. In contrast to EPCAM$^-$ tumour cells from *Lgr5-creER;Kras*^{G12D}*;p53*^{cKO}-derived SCCs that present full EMT, EPCAM$^-$ *Fat1*-cKO tumour cells continued to express high levels of several epithelial genes (such as *Krt14*, *p63* and *Sox2*). The transcriptional signature of *Fat1*-cKO tumour cells significantly overlapped with the hybrid EMT signature obtained by RNA-seq of CD106$^-$CD61$^-$CD51$^-$ hybrid EMT tumour cells from *Lgr5-creER;Kras*^{G12D}*;p53*^{cKO} SCCs and did not overlap significantly with the full EMT signature[11] (Fig. 3a, b, Extended Data Fig. 5f, g).

RNA-seq data from EPCAM$^+$ and EPCAM$^-$ *Fat1*-cKO lung cancer cells and from CRISPR–Cas9 *FAT1*-knockout human SCC cells showed that—in both cases—similar mesenchymal genes (including *ZEB1*, *ZEB2* and *VIM*) were upregulated following deletion of *FAT1*, uncovering a common gene signature associated with *FAT1* deletion across different tumour types and between mouse and human cancers. Importantly,

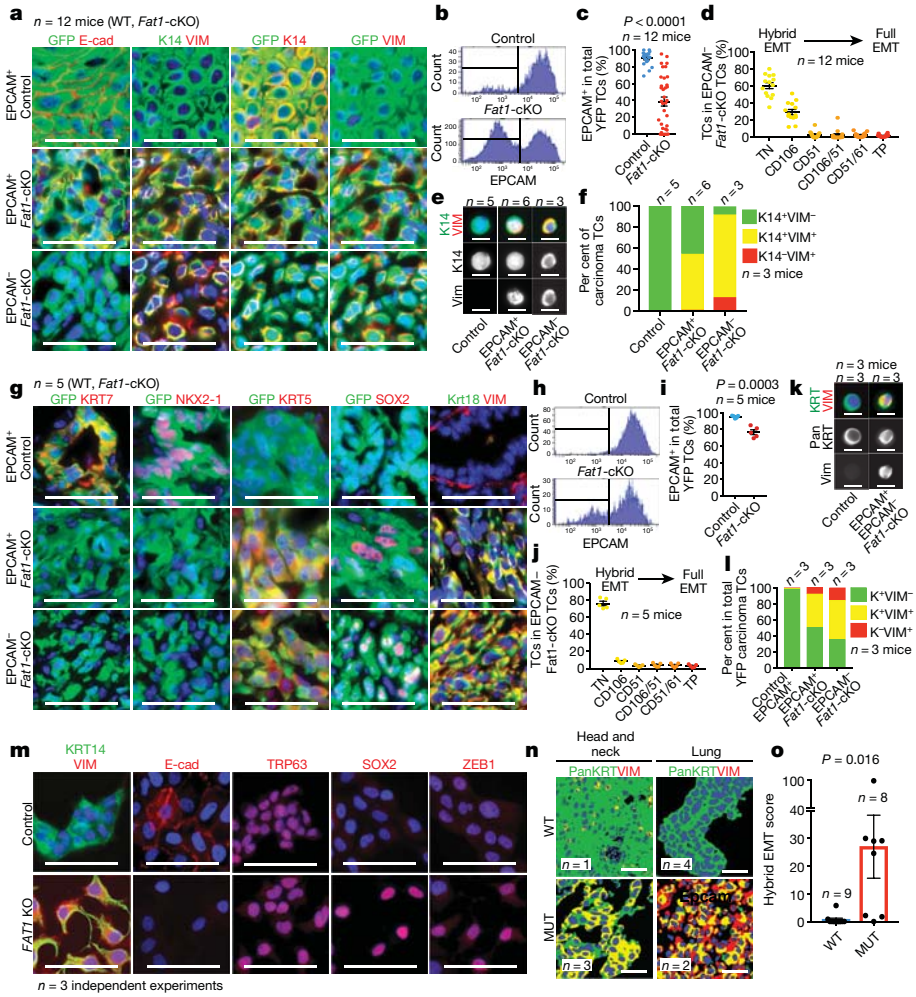

Fig. 1 | LOF of *Fat1* promotes hybrid EMT state in mouse skin SCC, mouse lung cancer and human SCC. a, Immunostaining for GFP, E-cadherin (E-cad), vimentin (VIM) and KRT14 (K14) in EPCAM$^+$ control (wild-type (WT)), EPCAM$^+$ *Fat1*-cKO and EPCAM$^-$ *Fat1*-cKO DMBA/TPA-induced SCCs. Scale bars, 50 µm. **b**, **c**, FACS analysis (**b**) and percentage of EPCAM expression (**c**) in control and *Fat1*-cKO YFP$^+$ skin SCCs. Mean ± s.e.m., two-tailed *t*-test. TC, tumour cell. **d**, Distribution of YFP$^+$EPCAM$^-$ tumour cells in CD106 (also known as VCAM1), CD61 (also known as ITGB3) and CD51 (also known as ITGAV) subpopulations in *Fat1*-cKO SCCs. Mean ± s.e.m. TN, EPCAM$^-$ triple negative (CD106$^-$CD51$^-$CD61$^-$); TP, EPCAM$^-$ triple positive (CD106$^+$CD51$^+$CD61$^+$). **e**, **f**, Co-immunostaining (**e**) and quantification (**f**) of KRT14 and vimentin in cytospin of FACS-isolated skin SCC tumour cells. Scale bars, 20 µm. *n* = 90 cells per condition and tumour. **g**, Immunostaining for GFP, KRT7, NKX2-1, KRT5, SOX2, KRT8 and KRT18 (KRT8/18), and vimentin in *Fat1* wild-type and -knockout lung carcinomas. Scale bars, 50 µm. **h**, **i**, FACS analysis (**h**) and percentage of EPCAM expression (**i**) in control and *Fat1*-cKO YFP$^+$ lung tumour cells. Mean ± s.e.m., two-tailed *t*-test. **j**, Distribution of YFP$^+$EPCAM$^-$ tumour cells in CD106/VCAM1, CD61/ITGB3 and CD51/ITGAV subpopulations in *Fat1*-cKO lung carcinomas. Mean ± s.e.m. **k**, **l**, Co-immunostaining (**k**) and quantification (**l**) of pancytokeratin (pan KRT) and vimentin in cytospin of FACS-isolated lung carcinoma tumour cells. Scale bars, 20 µm. *n* = 70 cells per condition and tumour. In **l**, K denotes pancytokeratin. **m**, Immunostaining for KRT14 and vimentin, E-cadherin, SOX2, TRP63 and ZEB1 in *FAT1* wild-type and *FAT1*-knockout (KO) A388 human skin SCC cell line. Scale bars, 50 µm. **n**, **o**, Representative images (**n**) and quantification of hybrid EMT score (**o**) (colocalization of pancytokeratin and vimentin) in wild-type and *FAT1*-mutated (MUT) head and neck, and lung, patient-derived xenografts. Scale bars, 50 µm, Mean ± s.e.m., two-tailed Mann–Whitney *U* test.

we found that high expression of this common *FAT1*-mutated signature was associated with poor survival in patients with lung SCC (Fig. 3c–e).

YAP1 and SOX2 regulate the hybrid EMT

To define the changes in the chromatin landscape that are responsible for the hybrid EMT state that occurs after deletion of *Fat1*, we performed assay for transposase-accessible chromatin using sequencing (ATAC-seq) of FACS-isolated wild-type and *Fat1*-cKO EPCAM$^+$ and EPCAM$^-$ tumour cells. We identified enhancers within key EMT transcription factors (such as *Zeb1*, *Snail1* or *Twist2*) and other EMT markers (for example, *Vim* or *Col6a3*) that were more accessible in EPCAM$^+$ *Fat1*-cKO tumour cells as compared to EPCAM$^+$ wild-type cells, which potentially accounts for the epigenetic priming of tumour cells to undergo EMT upon *Fat1* deletion. By performing motif discovery in differentially accessible chromatin regions between wild-type and *Fat1*-mutated tumour cells, we identified *Ap1* (also known as *Jun*) and Tead transcription-factor motifs as being strongly enriched in the chromatin regions that are more open in *Fat1*-mutated tumour cells that also have increased expression of YAP1 (Fig. 3f, Extended Data Fig. 6), which suggests that the JUN and FOS family of transcription factors cooperates with other transcription factors—including those of the TEAD family—that relay the YAP1 pathway to the nucleus to prime the *Fat1*-mutated cancer cells to undergo the EMT in skin SCC in vivo[8].

To identify the transcription factors that are responsible for the sustained expression of epithelial genes in EPCAM$^-$ *Fat1*-cKO tumour cells, we performed motif discovery in the ATAC-seq peaks that were upregulated in EPCAM$^-$ *Fat1*-cKO as compared to EPCAM$^-$ control

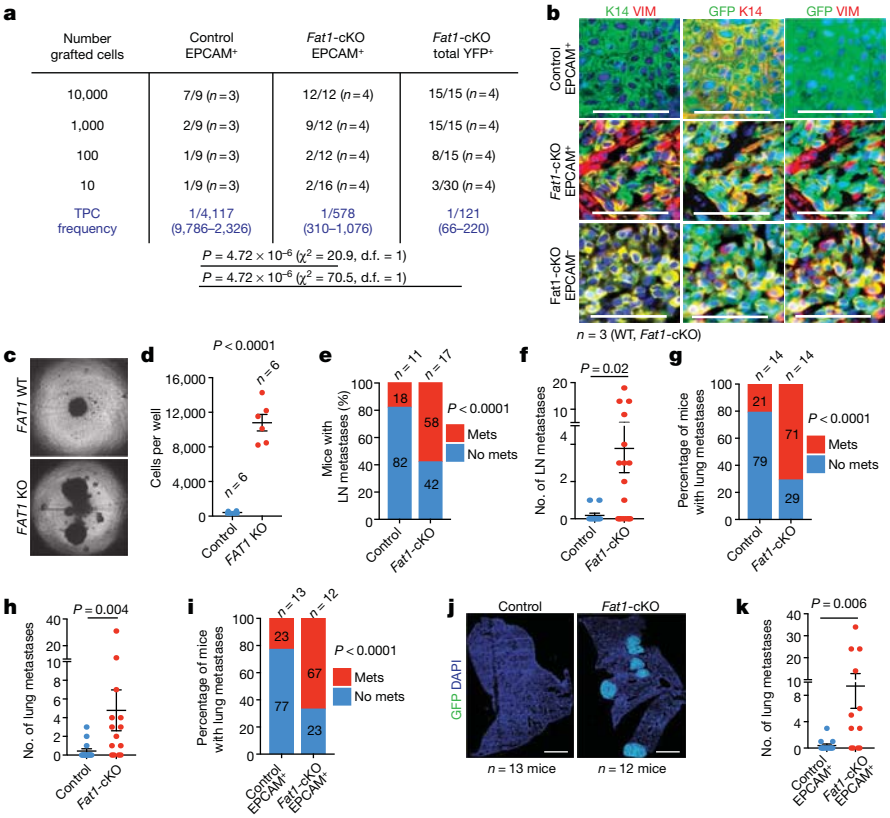

Fig. 2 | *Fat1* deletion promotes tumour stemness and metastasis in skin SCCs. a, Tumour-propagating cell (TPC) frequency observed upon subcutaneous transplantation of limiting dilutions of YFP$^+$EPCAM$^+$ control, YFP$^+$EPCAM$^+$ and total YFP$^+$ *Fat1*-cKO tumour cells using extreme limiting dilution analysis. χ^2 test. d.f., degrees of freedom. **b**, Immunostaining for GFP, KRT14 and vimentin in the secondary tumours arising after subcutaneous transplantation of tumour cells. Scale bars, 50 µm. **c**, Images showing spheroids formed 7 d after plating 4,000 *FAT1* wild-type or *FAT1*-knockout human A388 skin SCC cells on an ultra-low adherent plate. **d**, Quantification of cell number in *FAT1* wild-type and *FAT1*-knockout spheroids. Mean + s.e.m., two-tailed *t*-test. **e**, **f**, Proportion of mice presenting lymph node (LN) metastasis (χ^2 test) (**e**) and number of lymph node metastases per mouse (**f**) (mean ± s.e.m., two-tailed *t*-test). Mets, metastases. **g**, **h**, Proportion of mice presenting lung metastasis (χ^2 test) (**g**) and number of lung metastases per mouse (**h**) (mean ± s.e.m., two-tailed *t*-test). **i**, Proportion of mice presenting lung metastasis 40 d after intravenous injection of 20,000 YFP$^+$EPCAM$^+$ tumour cells. χ^2 test. **j**, Mosaic images of immunostaining for YFP of lungs after intravenous injection of control and *Fat1*-cKO tumour cells Scale bars, 1 mm. **k**, Number of metastases per lung arising from the injection of 20,000 YFP$^+$EPCAM$^+$ *Fat1* wild-type and *Fat1*-cKO tumour cells. Mean ± s.e.m., two-tailed *t*-test.

tumour cells from fully mesenchymal *Lgr5-creER;Kras^{G12D};p53^{cKO}* SCCs. We found that *Ap1*, Sox or Klf motifs were strongly enriched in EPCAM$^-$ *Fat1*-cKO cells (Fig. 3g, Extended Data Fig. 6), which suggests that the epithelial program of the hybrid EMT state in *Fat1*-cKO is mediated by an AP1–SOX2–KLF transcriptional network. *SOX2* is amplified in many human SCCs and marks cancer stem cells in skin SCCs[15–17], and could be responsible for the sustained expression of epithelial genes in *Fat1*-cKO tumour cells.

To functionally validate the bioinformatic predictions, we assessed the effect of CRISPR–Cas9-mediated deletion of *Yap1* and *Taz*, or of *Sox2*, on tumour stemness, metastasis and the gene expression program of mouse skin SCCs. Both tumour-propagating cell frequency and the number of metastasis were reduced upon deletion of *Sox2* or of *Yap1* and *Taz* in primary EPCAM$^-$ cell lines derived from *Lgr5-creER;Kras^{G12D};p53^{cKO};Fat^{cKO}* SCCs (Fig. 3h, i), which demonstrates that the SOX2 and the YAP1 and TAZ transcriptional programs are important for the promotion of tumour stemness and metastasis downstream of *Fat1* deletion. *SOX2* or *YAP1* deletion in the human SCC cell line decreased the tumour growth mediated by *FAT1* deletion in 3D spheroid assays (Fig. 3j), which demonstrates that SOX2 and YAP1 promote tumour growth downstream of *FAT1* deletion in human cancer cells. Conversely, the deletion of the E-cadherin gene (*CDH1*) in the same cell line—which induced defects of cell adhesion—did not induce SOX2 or ZEB1 expression, or an increase in nuclear YAP1. Overexpression of *CDH1* in *FAT1*-knockout cells did not decrease the clonogenicity or the expression of mesenchymal genes induced by *FAT1* deletion (Extended Data Fig. 7a–f), which shows that the promotion of tumour stemness or the hybrid EMT phenotype by *FAT1* deletion is not simply the result of a defect in cell adhesion.

Sox2 deletion in *Lgr5-creER;Kras^{G12D};p53^{cKO};Fat^{cKO}* SCCs resulted in the loss of epithelial characteristics and a shift from hybrid to complete EMT upon subcutaneous transplantation, whereas the deletion of *Yap1* and *Taz* promoted an early hybrid EMT state (as shown by immunostaining and FACS analysis) (Fig. 3k–m, Extended Data Fig. 7g–i). The RNA-seq data from *Fat1* and *Sox2* knockout further demonstrated a significant enrichment in the late EMT signature, marked by an increase of mesenchymal markers (for example, *Lox* and *Pdgfra*) and a decrease of epithelial markers (for example, *Cebpa*, *Krt5* and *p63*). Instead, the transcriptome of *Fat1*, *Yap1* and *Taz* triple-knockout SCCs showed significant enrichment of the EPCAM$^+$ epithelial and early hybrid EMT signature. Many classical canonical target genes of YAP1 and TAZ (for example, *Ctgf* (also known as *Ccn2*), *Amotl2* and *Fstl1*), as well as EMT genes (for example, *Vcam1*, *Thy1* and *Pdgfrb*), were decreased after *Fat1*, *Yap1* and *Taz* triple knockout as compared to *Fat1* knockout (Fig. 3n, o, Extended Data Fig. 7j, k and data not shown). Altogether, these data demonstrate that SOX2, and YAP1 and TAZ, control distinct transcriptional programs that lead to a stable hybrid EMT phenotype downstream of *Fat1* LOF.

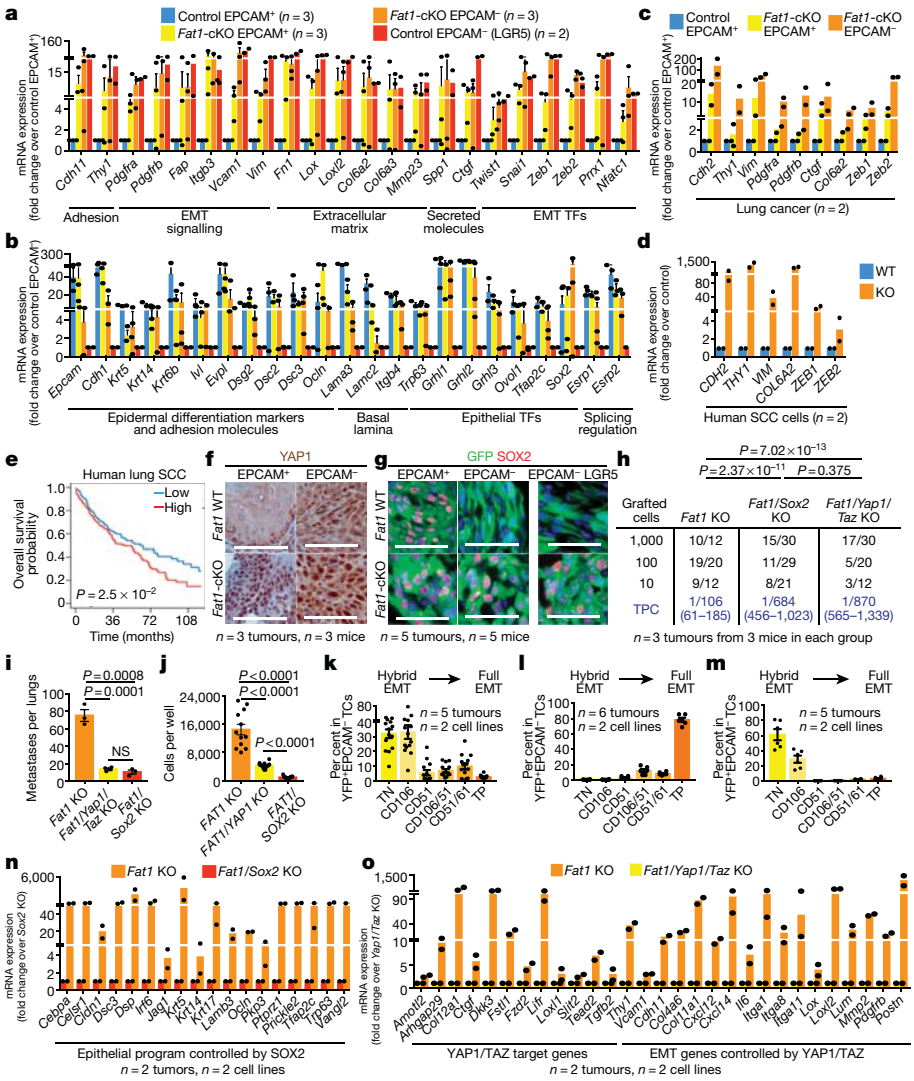

Fig. 3 | YAP1 and SOX2 regulate mesenchymal and epithelial states downstream of *Fat1* deletion. a, **b**, mRNA expression (RNA-seq) of mesenchymal (**a**) and epithelial (**b**) genes in mouse skin SCC. Mean + s.e.m. TF, transcription factor. **c**, **d**, mRNA expression (RNA-seq) of mesenchymal genes in mouse lung carcinoma (**c**) and human SCC cells (**d**). Mean + s.e.m. **e**, Overall survival of patients with lung SCC, stratified by the expression of the common gene signature between mouse skin and lung and human skin *FAT1*-knockout SCC. log-rank Mantel–Cox test. **f**, **g**, Immunohistochemistry for YAP1 (**f**) and immunostaining for GFP and SOX2 (**g**) in wild-type and *Fat1*-cKO skin SCCs. Scale bars, 50 µm. **h**, **i**, Tumour-propagating cells (**h**) and lung metastasis (**i**) following the injection of YFP$^+$EPCAM$^-$ *Fat1*-knockout, *Fat1*- and *Sox2* double-knockout or *Fat1*, *Yap1* and *Taz* triple-knockout skin SCC cells. Mean ± s.e.m. two-tailed-*t*-test. NS, not significant. **j**, Number of cells in spheroids formed by *FAT1*-knockout, *FAT1* and *YAP1* double-knockout or *FAT1* and *SOX2* double-knockout human SCC cells after 7 d. Mean ± s.e.m., two-tailed *t*-test. **k**–**m**, YFP$^+$EPCAM$^-$ CD106/VCAM1, CD61/ITGB3 and CD51/ITGAV subpopulations in SCC after subcutaneous transplantation of *Fat1*-cKO (**k**), *Fat1* and *Sox2* double-knockout (**l**) or *Fat1*, *Yap1* and *Taz* triple-knockout (**m**) mouse skin SCC cells. Mean ± s.e.m. Scale bars, 50 µm. **n**, **o**, mRNA (RNA-seq) expression of genes controlled by *Sox2* (**n**) or by *Yap1* and *Taz* (**o**) in EPCAM$^-$ *Fat1*-cKO skin SCC. Mean + s.e.m.

Signalling cascades downstream of *FAT1*

To understand how *FAT1* LOF activates SOX2 or YAP1 and TAZ, we performed a phosphoproteomic analysis of wild-type and CRISPR–Cas9 *FAT1*-knockout human SCC cells. We identified 288 phosphosites that were significantly upregulated and 335 that were significantly downregulated in *FAT1*-knockout tumour cells as compared to *FAT1* wild type. *FAT1* LOF induced a decrease in the phosphorylation of proteins involved in cell–cell adhesion (such as ZO1 or ZO2), as well as of PRKCD, EGFR, ERBB2, MEK1, MEK2, AKT2 or MTOR. In good accordance with the phosphoproteomic analysis, MEK1 and MEK2 were significantly less phosphorylated—and the total levels of EGFR and phosphorylated EGFR—were decreased in *FAT1*-knockout tumour cells (Fig. 4a–c, Extended Data Figs. 8, 9). These data suggest that EGFR–RAS–RAF–MEK–MAPK and the EGFR–PI3K–AKT–MTOR signalling pathways are decreased upon *FAT1* LOF.

Conversely, *FAT1*-deficient tumour cells exhibited a strong increase in the phosphorylation of the YES tyrosine kinase that belongs to the SRC family, as well as of the MAP1B and GJA1 proteins. GJA1 phosphorylation promotes GJA1 localization at the plasma membrane and increases the formation of functional gap junctions, which has previously been linked to increased metastatic capacity[18] (Extended Data Fig. 8). These data suggest that *FAT1* LOF induces a global remodelling of cell–cell adhesions, cell communication and the cytoskeleton, which is associated with the acquisition of a hybrid EMT state.

To decipher the signalling cascade that acts downstream of *FAT1* LOF, we used the PhosphoSitePlus online tool and bibliographic search to predict kinases that act upstream of the phosphosites we identified.

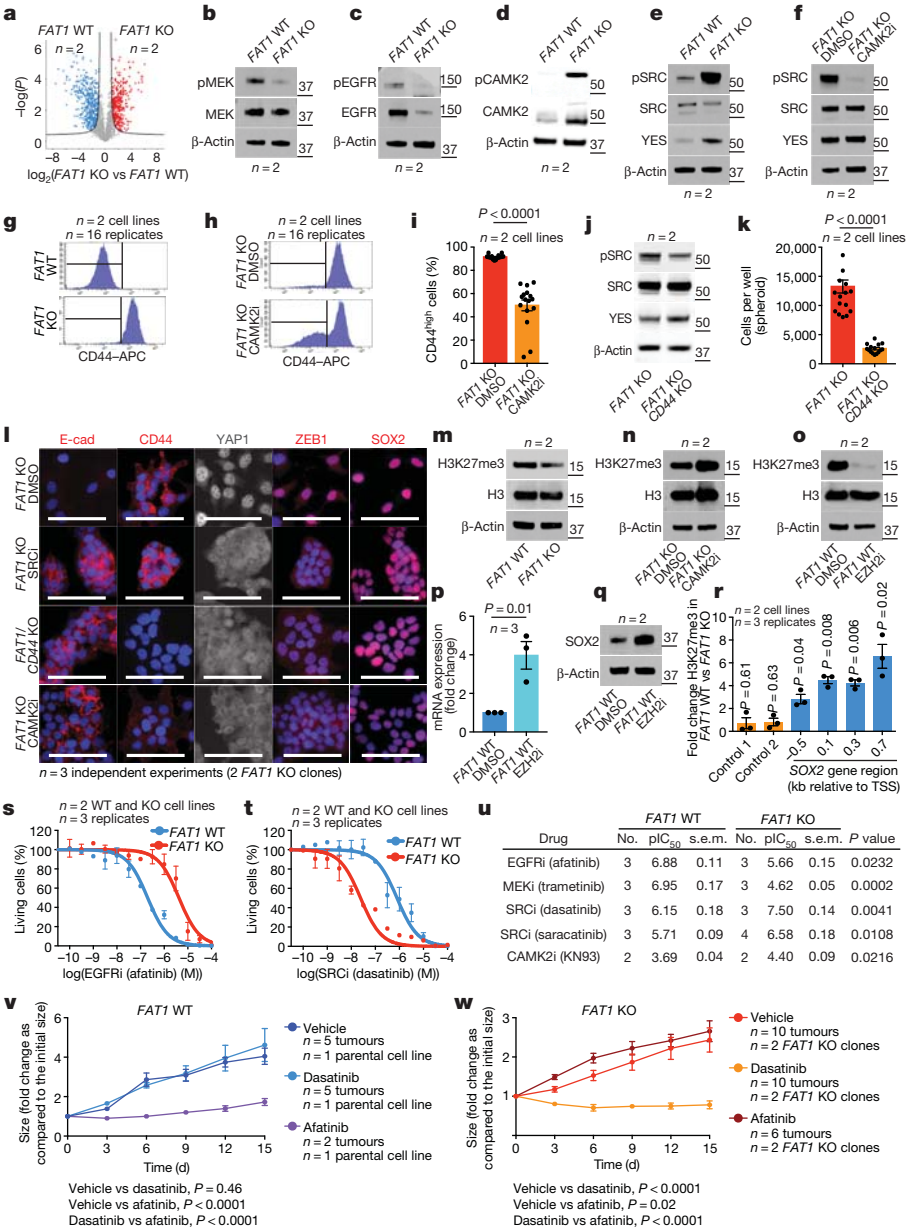

Drug	FAT1 WT No.	FAT1 WT pIC_{50}	FAT1 WT s.e.m.	FAT1 KO No.	FAT1 KO pIC_{50}	FAT1 KO s.e.m.	P value
EGFRi (afatinib)	3	6.88	0.11	3	5.66	0.15	0.0232
MEKi (trametinib)	3	6.95	0.17	3	4.62	0.05	0.0002
SRCi (dasatinib)	3	6.15	0.18	3	7.50	0.14	0.0041
SRCi (saracatinib)	3	5.71	0.09	4	6.58	0.18	0.0108
CAMK2i (KN93)	2	3.69	0.04	2	4.40	0.09	0.0216

Fig. 4 | Phosphoproteomic analysis identifies the signalling cascades downstream of *FAT1* deletion. a, Volcano plot showing the fold change and statistical significance of each phosphopeptide in wild-type versus *FAT1*-knockout cells (false-discovery rate (FDR) = 0.05, $S_0 = 1$). **b**–**e**, Western blot showing phosphorylated (p)MEK1 and MEK2 (MEK1/2) and total MEK (**b**), pEGFR and total EGFR (**c**), pCAMK2 and total CAMK2 (**d**), and pSRC, total SRC and YES (**e**) in *FAT1*-knockout and wild-type cells. **f**, Western blot showing pSRC, total SRC and YES in *FAT1*-knockout cells treated with dimethyl sulfoxide (DMSO) or with a CAMK2 inhibitor (CAMK2i). **g**, **h**, FACS analysis showing CD44 expression in wild-type and *FAT1*-knockout cells (**g**), and in *FAT1*-knockout cells treated with a CAMK2 inhibitor (**h**). **i**, *FAT1*-knockout cells expressing high levels of CD44 were treated with DMSO or a CAMK2 inhibitor. Mean + s.e.m. two-tailed *t*-test. **j**, Western blot showing pSRC, total SRC and YES in *FAT1*-knockout and *FAT1* and *CD44* double-knockout cells. **k**, Number of cells in *FAT1*-knockout and *FAT1* and *CD44* double-knockout spheroids. Mean + s.e.m. two-tailed *t*-test. **l**, Immunostaining for E-cadherin, CD44, YAP1, ZEB1 and SOX2 in *FAT1* and *CD44* double-knockout, and *FAT1*-knockout, cells treated with DMSO, an SRC inhibitor (SRCi) (saracatinib) or a CAMK2 inhibitor. Scale bars, 50 µm. **m**–**o**, Western blot showing the expression of H3K27me3 and total H3 in *FAT1* wild-type and -knockout cells (**m**), *FAT1*-knockout cells treated with a CAMK2 inhibitor (**n**) and in *FAT1* wild-type cells treated with DMSO or an EZH2 inhibitor (EZH2i) (**o**). **p**, **q**, *SOX2* mRNA (quantitative PCR with reverse transcription) (**p**) and protein (western blot) (**q**) in *FAT1* wild-type cells 7 d after treatment with an EZH2 inhibitor. Mean ± s.e.m., two-tailed *t*-test. **r**, ChIP–qPCR of H3K27me3 mark in regions close to the *SOX2* transcription start site. Ratio of relative enrichment in *FAT1* wild-type versus -knockout cells; one sample *t*-test, mean ± s.e.m. **s**, **t**, Dose–response curve showing the effect of the EGFR inhibitor (ECFRi) afatinib (**s**) and the SRC inhibitor dasatinib (**t**) on *FAT1* wild-type and *FAT1*-knockout cell viability at 48 h. Nonlinear regression log (inhibitor) with least-squares fit method. Mean ± s.e.m. **u**, Summary ($n = 3$) of pIC_{50} (negative log of half-maximal inhibitor concentration) and s.e.m. for different drugs for *FAT1* wild-type and *FAT1*-knockout cells. Two-tailed *t*-test. **v**, **w**, Effect of dasatinib and afatinib on *FAT1* wild-type (**v**) and *FAT1*-knockout (**w**) tumour growth upon subcutaneous transplantation. Mean ± s.e.m., two-way analysis of variance. The molecular weight (kDa) is indicated to the right of the blots in **b**–**f**, **j**, **m**–**o**, **q**.

Ca^{2+}/calmodulin-dependent protein kinase II (CAMK2) was the kinase that we found to most frequently act upstream of phosphopeptides enriched in *FAT1*-knockout tumour cells (CD44 on S706[19] and GJA1 on S328, S325, S306, S330, S364 and S365[20]). In accordance with the bioinformatic prediction, western blot analysis showed that CAMK2 was substantially more phosphorylated in *FAT1* LOF as compared to *FAT1*

wild type. We further confirmed that SRC and YES also showed high levels of expression and phosphorylation upon *FAT1* LOF. Immunoprecipitation of SRC and YES showed that YES was substantially more highly expressed and phosphorylated with *FAT1* knockout, whereas the levels of SRC were comparable between *FAT1* wild-type and -knockout tumour cells, and SRC phosphorylation was increased after *FAT1* knockout (Extended Data Fig. 8h). Treatment with a CAMK2 inhibitor (KN93) greatly decreased the level of SRC and YES phosphorylation, which shows that CAMK2 directly or indirectly phosphorylates YES and SRC upon *FAT1* LOF (Fig. 4d–f, Extended Data Fig. 8).

CD44 is upregulated during EMT, promoting tumour stemness, progression and metastasis[21]. Previous computational analysis predicted that an ESRP1–CD44–ZEB1 loop stabilizes the hybrid EMT state in human lung cancer cells[22]. Phosphorylation of CD44 by different kinases, including CAMK2[23], regulates its cellular localization and activity. To assess whether CD44 phosphorylation at S706 (which is upregulated upon *FAT1* LOF) could affect CD44 cellular localization, we performed a FACS analysis that revealed increased levels of cell-surface CD44 in *FAT1*-knockout cells, which were significantly reduced upon treatment with a CAMK2 inhibitor (Fig. 4g–i). To determine whether CAMK2 phosphorylates YES and SRC directly or through CD44[21] signalling in *FAT1*-knockout cells, we performed *CD44* deletion using CRISPR–Cas9 in *FAT1*-knockout cells and found that phosphorylation of SRC was decreased upon double knockout of *CD44* and *FAT1* (Fig. 4g–j). These data demonstrate that upon *FAT1* LOF, CAMK2 activates SRC at least partially though CD44. The clonogenicity of *FAT1* and *CD44* double-knockout human SCC cells decreased significantly in 3D tumour spheroid assays (Fig. 4k), which demonstrates that CD44 stabilization contributes to the increase in tumour stemness observed upon *FAT1* LOF.

We further assessed whether the hybrid EMT phenotype could be promoted by CAMK2–CD44–SRC signalling. We found that *FAT1* and *CD44* double-knockout and *FAT1*-knockout cells treated with CAMK2 (KN93) or SRC (saracatinib or dasatinib) inhibitors presented a strong decrease in nuclear YAP1 and ZEB1 and an increase in expression of E-cadherin, and were growing in more-compact epithelial colonies. These results demonstrate that *FAT1* LOF activates a CAMK2–CD44–SRC–YAP–ZEB1 axis that promotes the expression of a mesenchymal program. We observed a decrease in SOX2 expression only in *FAT1*-knockout tumour cells treated with a CAMK2 inhibitor. However, no change in SOX2 expression was observed upon inhibition of the CD44–SRC cascade (Fig. 4l).

Phosphoproteomic analysis revealed an increase in the inactivating phosphorylation of EZH2 at T487[24] in *FAT1*-knockout cells. EZH2 belongs to the PRC2 complex that methylates H3 at K27, mediating transcriptional repression[25]. This histone mark is remodelled at the *Sox2* locus during the formation of SCCs[15]. We hypothesized that EZH2 inhibition in *FAT1*-knockout cells could decrease trimethylation of H3 at K27 (H3K27me3) repressive histone marks, and thus promote the expression of *SOX2*. The global level of H3K27me3 was substantially decreased in *FAT1*-knockout cells, which suggests that EZH2 could be less active upon *FAT1* LOF. Administration of a CAMK2 inhibitor increased the global levels of H3K27me3 in *FAT1*-knockout cells, consistent with the notion that CAMK2 activation inhibits EZH2 and PRC2 activity in tumour cells. To further validate this hypothesis, we treated *FAT1* wild-type cells with an EZH2 inhibitor (GSK343) and observed a decrease of H3K27me3 and increase in SOX2 mRNA and protein expression after seven days of treatment, which further suggests that SOX2 is epigenetically regulated by a FAT1–CAMK2–EZH2-dependent mechanism. Chromatin immunoprecipitation with quantitative PCR (ChIP–qPCR) demonstrated that H3K27me3 marks around the *SOX2* promoter were significantly reduced upon *FAT1* deletion, which provides support for the notion that *FAT1* deletion regulates the expression of SOX2 through an epigenetic mechanism (Fig. 4m–r).

As YAP1 and TAZ signalling can be regulated by the stiffness of the extracellular matrix[26], we assessed the effect of substrate stiffness on YAP1 and SOX2 expression. In contrast to *FAT1* wild-type cells, *FAT1*-knockout tumour cells exhibited high levels of total and nuclear YAP1 expression even on a soft substrate, which demonstrates that *FAT1* deletion constitutively activates signalling pathways that lead to high YAP1 expression; this causes the *FAT1*-knockout cells to behave—in respect to YAP1 nuclear expression—as if the tumour cells were exposed to a stiff substrate. No changes in SOX2 expression were observed, demonstrating that SOX2 is constitutively activated upon *FAT1* LOF independently of the extracellular stiffness (Extended Data Fig. 10a–d).

Drug vulnerabilities in *FAT1*-mutated tumours

To test whether the signalling cascades that change upon *FAT1* LOF could predict therapeutic resistance and vulnerability of *FAT1*-mutated cancers, we assessed the sensitivity of wild-type and isogenic *FAT1*-knockout human cancer cell lines to the inhibitors of the signalling pathways that we found to be differentially regulated between wild-type and *FAT1*-knockout cells. EGFR inhibitors such as afatinib, and MEK inhibitors such as trametinib, are widely used in patients with metastatic SCC[27,28]. *FAT1*-knockout cells were significantly more resistant to afatinib and trametinib as compared to *FAT1* wild-type SCC cells in vitro (Fig. 4s–u).

By contrast, *FAT1*-knockout tumour cells were significantly more sensitive to the SRC inhibitors dasatinib and saracatinib and the CAMK2 inhibitor KN93 as compared to *FAT1* wild-type tumour cells (Fig. 4s–u). Administration of afatinib and dasatinib to mice transplanted with *FAT1* wild-type and -knockout human SCC cell lines showed that *FAT1* wild-type tumour cells were more sensitive to afatinib and *FAT1*-knockout tumour cells were more sensitive to dasatinib (Fig. 4v, w), consistent with the difference in drug sensitivity observed in vitro.

Discussion

Our study reveals that, in mouse models and human cancers, *FAT1* deletion promotes the acquisition of a hybrid EMT state that presents increased tumour stemness and metastasis. We identify the epigenetic and transcriptional mechanisms that link a loss of cell polarity and cell adhesion with the induction of a hybrid EMT phenotype downstream of *Fat1* deletion. Our comprehensive molecular characterization—including transcriptomic, epigenomic and proteomic characterization of *Fat1* mutants—shows that the hybrid EMT signature is mediated by the activation of YAP1 and SOX2, which regulate the co-expression of mesenchymal and epithelial transcriptional programs, respectively, in cancer cells. We show that the gene signature associated with *FAT1* LOF is predictive of poor survival in patients with lung cancer. We identify the signalling cascades that lead to the activation of YAP1 and SOX2 downstream of *FAT1* LOF. The activation and inhibition of these signalling pathways lead to an increased sensitivity of *FAT1*-mutated cancer cells to CAMK2 and SRC inhibition and to resistance to EGFR and MEK inhibition (Extended Data Fig. 10). This study has important implications for personalized medicine, in the prognosis and treatment of the high number of patients with cancer that displays *FAT1* mutations.

Online content

Any methods, additional references, Nature Research reporting summaries, source data, extended data, supplementary information, acknowledgements, peer review information; details of author contributions and competing interests; and statements of data and code availability are available at https://doi.org/10.1038/s41586-020-03046-1.

1. Morris, L. G. et al. Recurrent somatic mutation of FAT1 in multiple human cancers leads to aberrant Wnt activation. *Nat. Genet.* **45**, 253–261 (2013).
2. Dotto, G. P. & Rustgi, A. K. Squamous cell cancers: a unified perspective on biology and genetics. *Cancer Cell* **29**, 622–637 (2016).
3. Sánchez-Danés, A. & Blanpain, C. Deciphering the cells of origin of squamous cell carcinomas. *Nat. Rev. Cancer* **18**, 549–561 (2018).

4. The ICGC/TCGA Pan-Cancer Analysis of Whole Genomes Consortium. Pan-cancer analysis of whole genomes. *Nature* **578**, 82–93 (2020).
5. Lawrence, M. S. et al. Discovery and saturation analysis of cancer genes across 21 tumour types. *Nature* **505**, 495–501 (2014).
6. Li, Z. et al. Loss of the FAT1 tumor suppressor promotes resistance to CDK4/6 inhibitors via the Hippo pathway. *Cancer Cell* **34**, 893–905.e8 (2018).
7. Nassar, D., Latil, M., Boeckx, B., Lambrechts, D. & Blanpain, C. Genomic landscape of carcinogen-induced and genetically induced mouse skin squamous cell carcinoma. *Nat. Med.* **21**, 946–954 (2015).
8. Martin, D. et al. Assembly and activation of the Hippo signalome by FAT1 tumor suppressor. *Nat. Commun.* **9**, 2372 (2018).
9. Hu, X. et al. FAT1 prevents epithelial mesenchymal transition (EMT) via MAPK/ERK signaling pathway in esophageal squamous cell cancer. *Cancer Lett.* **397**, 83–93 (2017).
10. Srivastava, C. et al. FAT1 modulates EMT and stemness genes expression in hypoxic glioblastoma. *Int. J. Cancer* **142**, 805–812 (2018).
11. Pastushenko, I. et al. Identification of the tumour transition states occurring during EMT. *Nature* **556**, 463–468 (2018).
12. Latil, M. et al. Cell-type-specific chromatin states differentially prime squamous cell carcinoma tumor-initiating cells for epithelial to mesenchymal transition. *Cell Stem Cell* **20**, 191–204.e5 (2017).
13. Pastushenko, I. & Blanpain, C. EMT transition states during tumor progression and metastasis. *Trends Cell Biol.* **29**, 212–226 (2019).
14. Nieto, M. A., Huang, R. Y., Jackson, R. A. & Thiery, J. P. EMT: 2016. *Cell* **166**, 21–45 (2016).
15. Boumahdi, S. et al. SOX2 controls tumour initiation and cancer stem-cell functions in squamous-cell carcinoma. *Nature* **511**, 246–250 (2014).
16. Ferone, G. et al. SOX2 is the determining oncogenic switch in promoting lung squamous cell carcinoma from different cells of origin. *Cancer Cell* **30**, 519–532 (2016).
17. Siegle, J. M. et al. SOX2 is a cancer-specific regulator of tumour initiating potential in cutaneous squamous cell carcinoma. *Nat. Commun.* **5**, 4511 (2014).
18. Cooper, C. D. & Lampe, P. D. Casein kinase 1 regulates connexin-43 gap junction assembly. *J. Biol. Chem.* **277**, 44962–44968 (2002).
19. Lewis, C. A., Townsend, P. A. & Isacke, C. M. Ca^{2+}/calmodulin-dependent protein kinase mediates the phosphorylation of CD44 required for cell migration on hyaluronan. *Biochem. J.* **357**, 843–850 (2001).
20. Huang, R. Y. et al. Identification of CaMKII phosphorylation sites in connexin43 by high-resolution mass spectrometry. *J. Proteome Res.* **10**, 1098–1109 (2011).
21. Chen, C., Zhao, S., Karnad, A. & Freeman, J. W. The biology and role of CD44 in cancer progression: therapeutic implications. *J. Hematol. Oncol.* **11**, 64 (2018).
22. Jolly, M. K. et al. Interconnected feedback loops among ESRP1, HAS2, and CD44 regulate epithelial–mesenchymal plasticity in cancer. *APL Bioeng.* **2**, 031908 (2018).
23. Chellaiah, M. A., Biswas, R. S., Rittling, S. R., Denhardt, D. T. & Hruska, K. A. Rho-dependent Rho kinase activation increases CD44 surface expression and bone resorption in osteoclasts. *J. Biol. Chem.* **278**, 29086–29097 (2003).
24. Göllner, S. et al. Loss of the histone methyltransferase EZH2 induces resistance to multiple drugs in acute myeloid leukemia. *Nat. Med.* **23**, 69–78 (2017).
25. Avgustinova, A. & Benitah, S. A. Epigenetic control of adult stem cell function. *Nat. Rev. Mol. Cell Biol.* **17**, 643–658 (2016).
26. Panciera, T., Azzolin, L., Cordenonsi, M. & Piccolo, S. Mechanobiology of YAP and TAZ in physiology and disease. *Nat. Rev. Mol. Cell Biol.* **18**, 758–770 (2017).
27. Machiels, J. P. et al. Afatinib versus methotrexate as second-line treatment in patients with recurrent or metastatic squamous-cell carcinoma of the head and neck progressing on or after platinum-based therapy (LUX-Head & Neck 1): an open-label, randomised phase 3 trial. *Lancet Oncol.* **16**, 583–594 (2015).
28. Planchard, D. et al. Dabrafenib plus trametinib in patients with previously untreated $BRAF^{V600E}$-mutant metastatic non-small-cell lung cancer: an open-label, phase 2 trial. *Lancet Oncol.* **18**, 1307–1316 (2017).

[1]Laboratory of Stem Cells and Cancer, Université Libre de Bruxelles (ULB), Brussels, Belgium. [2]Dermatology Department, Cliniques de l'Europe, Brussels, Belgium. [3]Dermatology Department, CHU Brugmann, Université Libre de Bruxelles (ULB), Brussels, Belgium. [4]Laboratory of Protein Phosphorylation and Proteomics, Department of Cellular and Molecular Medicine, KU Leuven, Leuven, Belgium. [5]Leuven Cancer Institute (LKI), Leuven, Belgium. [6]VIB Center for Medical Biotechnology, Ghent, Belgium. [7]VIB Proteomics Core, Ghent, Belgium. [8]Department of Biomolecular Medicine, Ghent University, Ghent, Belgium. [9]Alvéole, Paris, France. [10]CytoMorpho Lab, UMR976 HIPI, CEA, INSERM, Université de Paris, Paris, France. [11]CytoMorpho Lab, UMR5168 LPCV, CEA, CNRS, Université Grenoble-Alpes, Grenoble, France. [12]Breast Cancer Translational Research Laboratory J.-C. Heuson, Institut Jules Bordet, Université Libre de Bruxelles (ULB), Brussels, Belgium. [13]Center for Microscopy and Molecular Imaging (CMMI), Université Libre de Bruxelles (ULB), Charleroi, Belgium. [14]DIAPath, Center for Microscopy and Molecular Imaging, Université Libre de Bruxelles (ULB), Charleroi, Belgium. [15]Laboratory of Image Synthesis and Analysis, Ecole Polytechnique de Bruxelles, Université Libre de Bruxelles (ULB), Brussels, Belgium. [16]Department of Thoracic Surgery, Erasme University Hospital, Université Libre de Bruxelles (ULB), Brussels, Belgium. [17]Department of Otolaryngology – Head and Neck Surgery, Erasme University Hospital, Université Libre de Bruxelles (ULB), Brussels, Belgium. [18]Department of Dermatology, Complejo Asistencial Universitario de León, León, Spain. [19]Department of Otolaryngology – Head and Neck Surgery, Hospital Clinico 'Lozano Blesa', Zaragoza, Spain. [20]Dermatology Department, Ramón y Cajal Hospital, Madrid, Spain. [21]University of Alcalá, Madrid, Spain. [22]Instituto Ramón y Cajal de Investigación Sanitaria (IRyCIS), Madrid, Spain. [23]Department of Dermatology, Clinica Universidad de Navarra, Navarra, Spain. [24]Department of Maxillofacial Surgery, Head and Neck Surgery, Hospital Clínic, Barcelona, Spain. [25]Department of Dermatology, Hospital Costa del Sol, Marbella, Spain. [26]Department of Dermatology, Instituto Valenciano de Oncologia, Valencia, Spain. [27]Pathology Department, Erasme Hospital, Université Libre de Bruxelles (ULB), Brussels, Belgium. [28]Laboratory of Molecular Parasitology, IBMM, Université Libre de Bruxelles (ULB), Charleroi, Belgium. [29]Aix-Marseille Univ, CNRS, IBDM - UMR, 7288, Marseille, France. [30]WELBIO, Université Libre de Bruxelles (ULB), Brussels, Belgium. [31]These authors contributed equally: Ievgenia Pastushenko, Federico Mauri. ✉e-mail: Cedric.Blanpain@ulb.ac.be

Reporting summary

Further information on research design is available in the Nature Research Reporting Summary linked to this paper.

Data availability

All the raw sequencing data have been deposited in the Gene Expression Omnibus with the following accession numbers: mouse RNA-seq (GSE158502), human RNA-seq (GSE158501), ATAC-seq (GSE158501), whole-exome sequencing (GSE158503), low-coverage whole-genome sequencing (GSE158505) or a global accession number (GSE158506. The mass spectrometry proteomics data have been deposited to the ProteomeXchange Consortium via the PRIDE partner repository with the dataset identifier PXD022268. All other relevant data are available from the corresponding author upon reasonable request. Source data are provided with this paper.

Acknowledgements We thank the ULB animal facility and ULB genomic core facility (F. Libert and A. Lefort); and J. Allard from CMMI (supported by the European Regional Development Fund and the Walloon Region). I.P. is supported by FNRS and Foundation Against Cancer (FCC). F.M. was supported by FNRS post-doctoral fellowship and by the TELEVIE. The Department of Pathology (Erasme Hospital, ULB) acknowledges Fonds Yvonne Boel. C. Decaestecker is a senior research associate in F.R.S.-FNRS. The patient-derived xenograft project was supported by Fonds Erasme. C. Blanpain is supported by WELBIO, FNRS, Fond Erasme, Fondation Contre le Cancer, ULB Foundation, European Research Council, Worldwide Cancer Research and the Foundation Baillet Latour.

Author contributions I.P., F.M. and C. Blanpain designed the experiments and performed data analysis. I.P. and F.M. performed most of the biological experiments. F.H. generated *Fat1*-cKO mice and provided her expertise. Y. Song performed bioinformatic analysis. F.d.C. and B.S. helped to perform CRISPR experiments. B.M. and V.J. performed intratracheal AdenoCRE installation for lung cancer generation. F.I. and D.V.H. performed phosphoproteomic analysis. M.O. and M.T. performed stiffness experiments. M.V. and D.P.-M. performed electron microscopy imaging and analysis. F.I. and D.V.H. performed phosphoproteomic analysis. Y.B. and C.S. performed analysis of patient survival using the TCGA database. I.S., Y. Sokolow, S.H., A.P.-B., B.A.-M., L.R.-B., P.J., M.D.T., P.R., R.S.-G., N.D'H., J.F.M.-C. and O.S. provided human samples. C. Balsat, C. Decaestecker and Y.-R.V.E. performed staining and analysis of patient-derived xenograft samples. C. Dubois performed FACS. V.M., S.L., G.L., J.B., M.R. and S.S. performed immunostainings, western blotting, treatments and follow-up of the mice. All authors read and approved the final manuscript.

Competing interests C. Blanpain, I.P. and F.M. are co-inventors on a patent application on the use of SRC inhibitors for the treatment of *FAT1*-mutated cancers.

Additional information

Supplementary information The online version contains supplementary material available at https://doi.org/10.1038/s41586-020-03046-1.

Correspondence and requests for materials should be addressed to C.B.

Peer review information *Nature* thanks Salvador Aznar Benitah and the other, anonymous, reviewer(s) for their contribution to the peer review of this work.

a

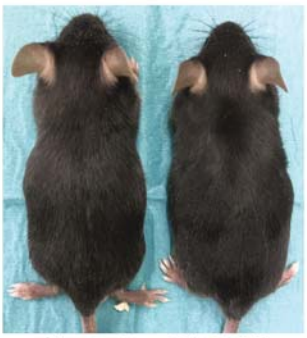

Control Fat1cKO

b

Birth rate

K14Cre(het);Fat1cKO x Fat1cKO

	#Mice	%Mice
Expected Control	84	50.0%
Expected Fat1cKO	84	50.0%
Observed Control	83	49.4%
Observed Fat1cKO	85	50.6%

n=168 mice, n=15 litters

c

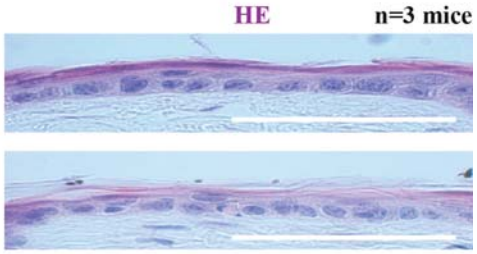

d

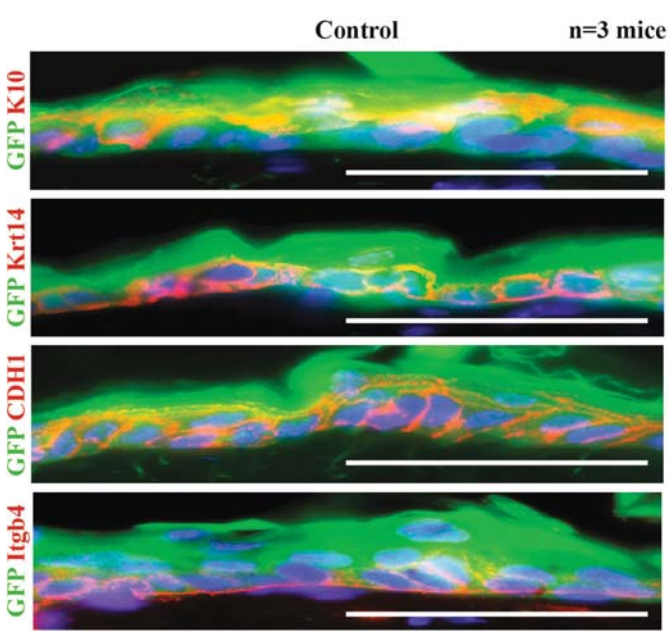

e

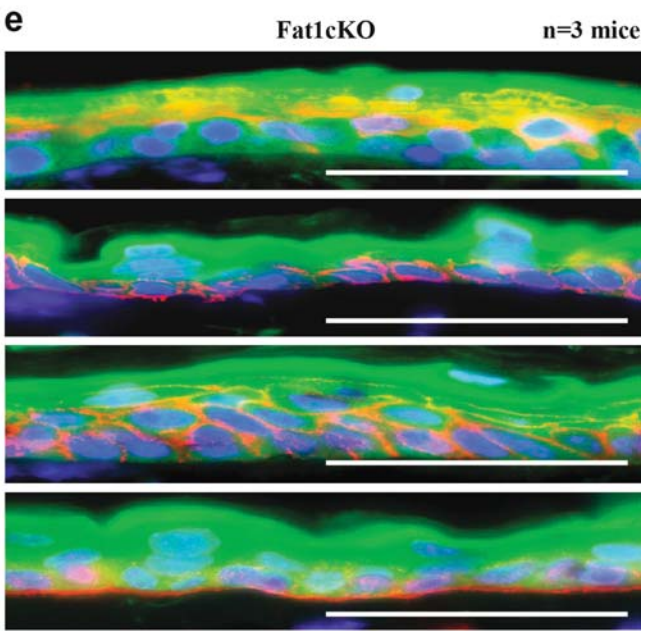

Extended Data Fig. 1 | *Fat1* LOF does not alter development and skin homeostasis. a, Image showing *Fat1*-cKO mouse and its control littermate. **b**, Table showing the number of control mice and mice with constitutive *Fat1*-cKO in skin epidermis, showing the absence of deviation from Mendelian ratio. **c**, Haematoxylin and eosin staining in control and *Fat1*-cKO epidermis. Scale bar, 50 µm. **d**, **e**, Immunostaining for GFP and KRT10, KRT14, E-cadherin or ITGB4 in control (**d**) and *Fat1*-cKO (**e**) epidermis. Scale bar, 50 µm.

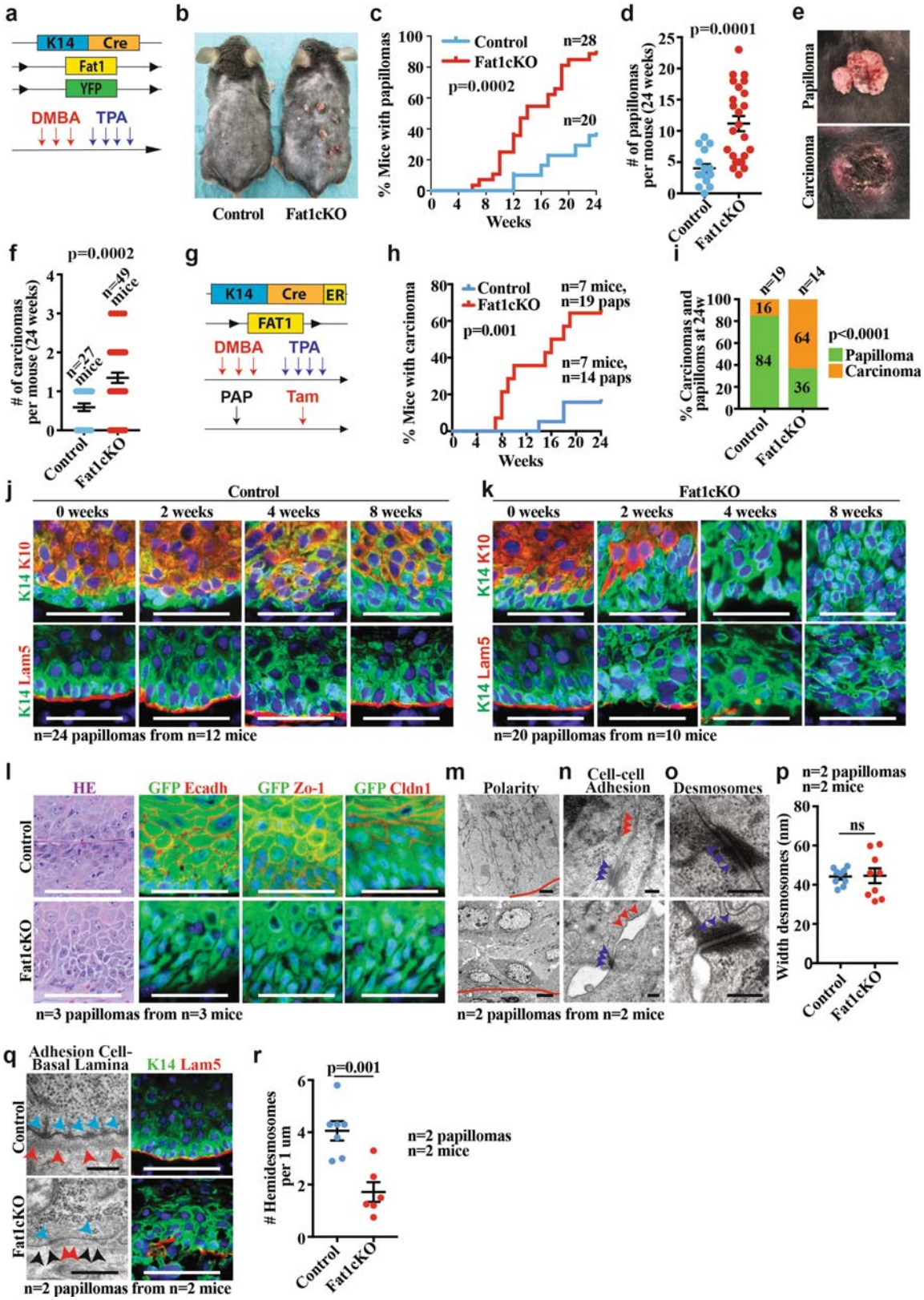

Extended Data Fig. 2 | See next page for caption.

Extended Data Fig. 2 | *Fat1* LOF accelerates DMBA/TPA-induced tumour initiation and malignant progression. a, Model allowing constitutive *Fat1* deletion in the skin epidermis and the scheme of DMBA/TPA protocol. **b**, Control and *Fat1*-cKO littermates 24 weeks after initiation of DMBA/TPA treatment. **c**, **d**, Time elapsed from the beginning of DMBA/TPA treatment until the appearance of the tumour (log-rank Mantel–Cox test) (**c**) and the number of papillomas per mouse (mean ± s.e.m., two-tailed *t*-test) (**d**) in control and *Fat1*-cKO mice. **e**, Macroscopic appearance of papilloma and carcinoma. **f**, Number of carcinomas per mouse at 24 weeks after DMBA/TPA in control and *Fat1*-knockout mice. Mean ± s.e.m., two-tailed *t*-test. **g**, Acute deletion of *Fat1* in DMBA/TPA-induced papillomas. **h**, Time elapsed from tamoxifen (tam) administration to macroscopic malignant progression from papillomas into carcinomas. log-rank Mantel–Cox test. **i**, Proportion of papillomas that progressed to carcinomas in control and *Fat1*-cKO mice. χ^2 test. **j**, **k**, Immunostaining for KRT14, KRT10 and LAM5 in control (**j**) and *Fat1*-cKO papillomas (**k**) 0, 2, 4 and 8 weeks after tamoxifen administration. Scale bar, 50 µm. **l**, Haematoxylin and eosin and immunostaining for YFP, E-cadherin, ZO-1 or CLDN1 in control and *Fat1*-cKO papillomas. Scale bar, 50 µm. **m**–**o**, Electron microscopy images showing polarity (Scale bars, 2 µm (control papilloma), 5 µm (*Fat1*-cKO papilloma)) (**m**), cell–cell adhesion (scale bar, 0.2 µm) (**n**) or desmosomes (scale bar, 0.2 µm) (**o**) in *Fat1*-cKO and wild-type papillomas. Red lines indicate interface between tumour cells and stroma. Blue arrowheads, desmosomes. Red arrowheads, tight and adherens junctions. **p**, Width of the desmosomes measured in nm in control and *Fat1*-cKO papillomas. Mean ± s.e.m., two-tailed *t*-test. **q**, Electron microscopy (scale bars, 0.2 µm (control), 5 µm (*Fat1*-cKO)) and immunostaining for KRT14 and LAM5 (scale bar, 50 µm) of control and *Fat1*-cKO papillomas. Blue arrowheads, hemidesmosomes. Red arrowheads, basal lamina in control papillomas and discontinued basal lamina in *Fat1*-cKO papillomas. Black arrowheads show fenestration of basal lamina in *Fat1*-cKO papillomas. **r**, Number of hemidesmosomes per 1 µm. Mean ± s.e.m., two-tailed *t*-test).

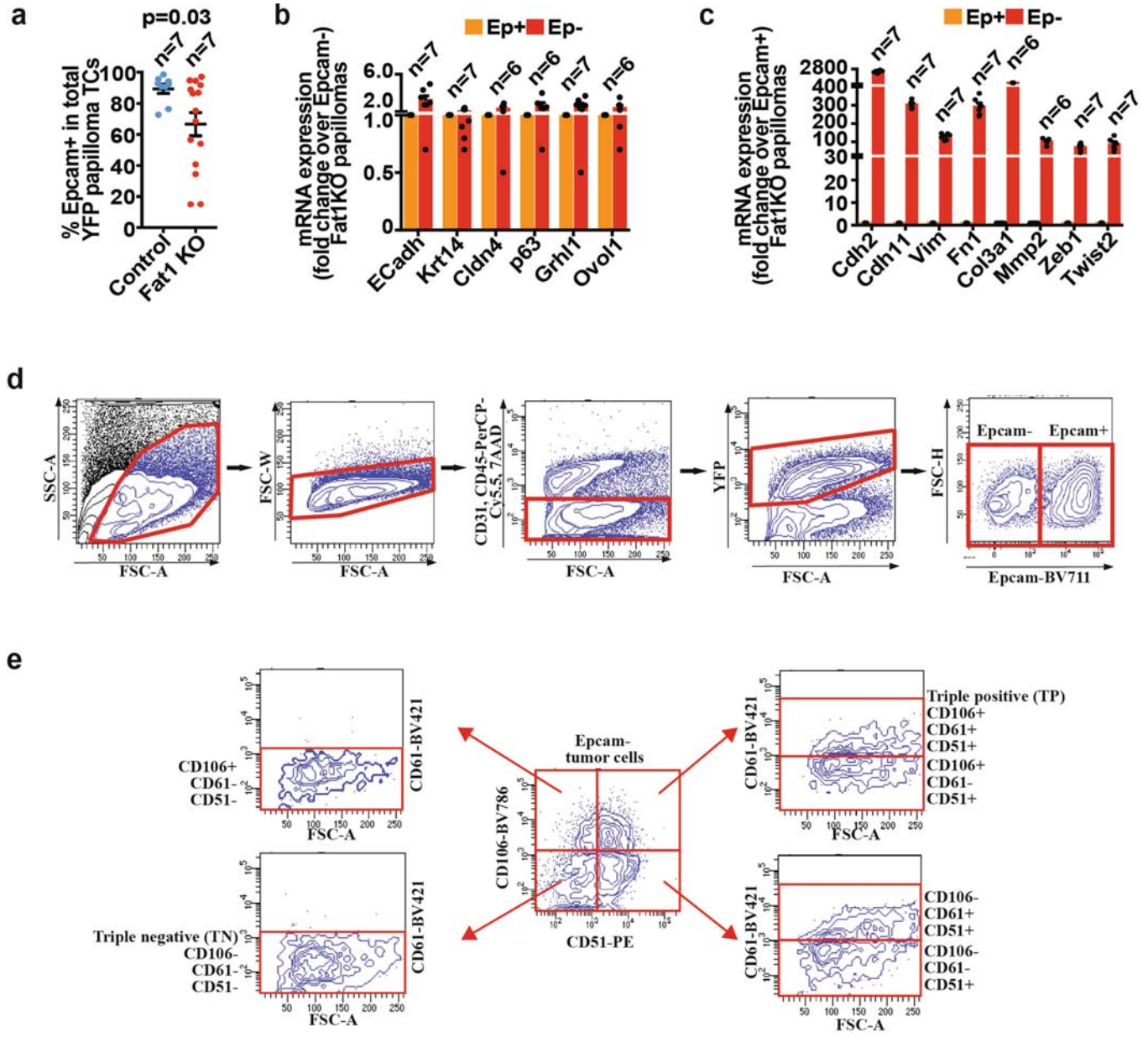

Extended Data Fig. 3 | EMT in papillomas and gating strategy for FACS analysis and cell sorting of the tumour subpopulations. a, Percentage of EPCAM$^+$YFP$^+$ tumour cells in control and *Fat1*-cKO papillomas. Mean ± s.e.m., two-tailed *t*-test. **b**, **c**, mRNA (qPCR) expression of epithelial (**b**) and mesenchymal (**c**) genes in EPCAM$^+$ and EPCAM$^-$ control and *Fat1*-cKO papillomas. Mean + s.e.m. **d**, FACS plots showing the gating strategy used to FACS-isolate or to analyse the proportion of YFP$^+$EPCAM$^+$ and EPCAM$^-$ tumour cells from DMBA/TPA-induced *K14-cre;Fat1^{cKO};Rosa26$^{YFP/+}$* carcinomas and papillomas, *Lgr5-creER;KRas^{G12D};p53^{cKO};Fat1^{cKO};Rosa26$^{YFP/+}$* or *K14-creER;KRas^{G12D};p53^{cKO};Fat1^{cKO};Rosa26$^{YFP/+}$* skin SCCs and *Kras^{G12D};p53^{cKO};Fat1^{cKO};Rosa26$^{YFP/+}$* lung carcinomas. **e**, FACS plots showing the gating strategy to define the six subpopulations of EPCAM$^-$ tumour cells: EPCAM$^-$CD106$^-$CD51$^-$CD61$^-$ (triple negative), EPCAM$^-$CD106$^+$CD51$^-$CD61$^-$, EPCAM$^-$CD106$^-$CD51$^+$CD61$^-$, EPCAM$^-$CD106$^+$CD51$^+$CD61$^-$, EPCAM$^-$CD106$^-$CD51$^+$CD61$^+$ and EPCAM$^-$CD106$^+$CD51$^+$CD61$^+$ (triple positive) populations.

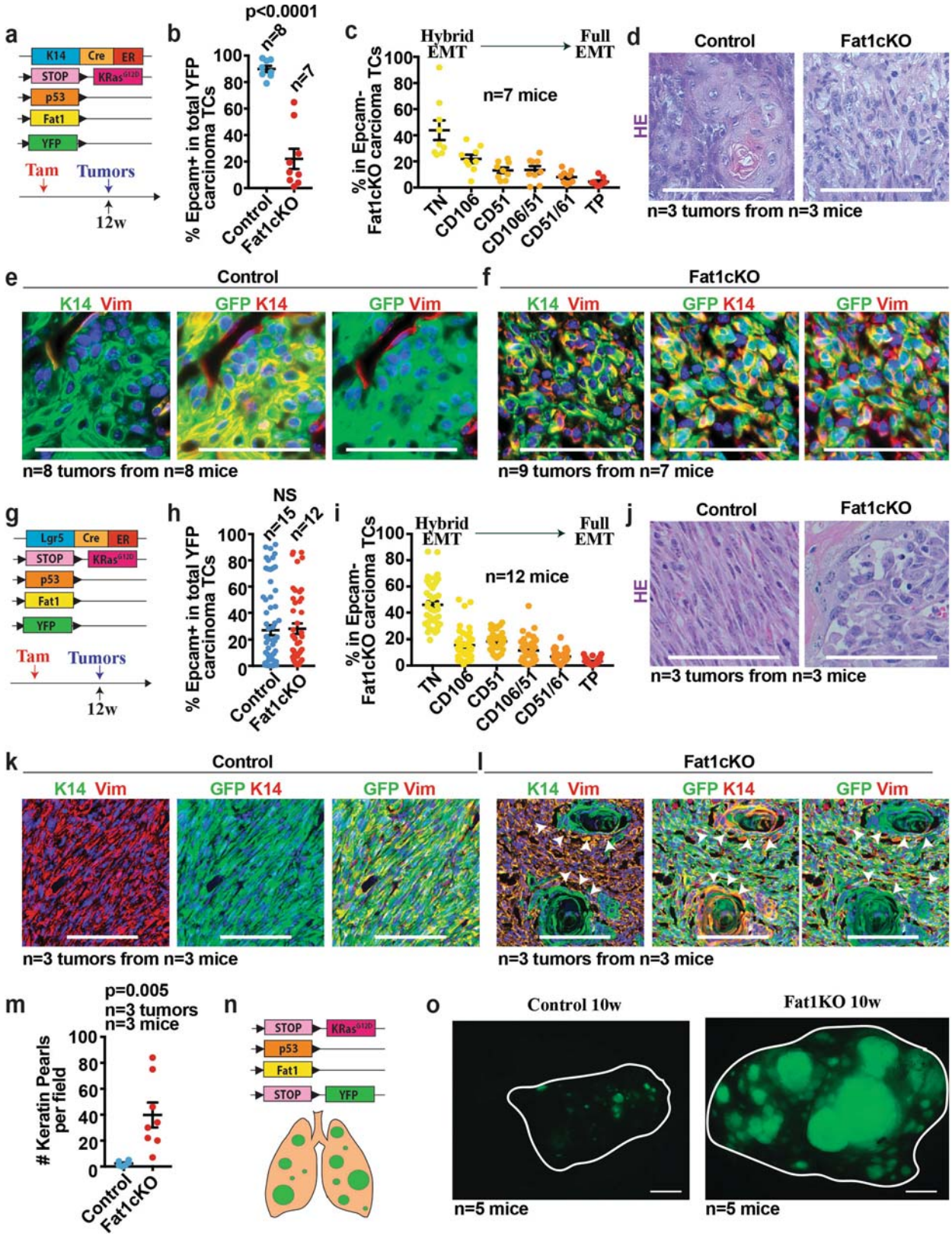

Extended Data Fig. 4 | See next page for caption.

Extended Data Fig. 4 | *Fat1* LOF promotes hybrid EMT state in a genetic model of skin SCC. a, Mouse model of skin SCC allowing YFP and $Kras^{G12D}$ expression as well as *p53* and *Fat1* deletion preferentially in the interfollicular epidermis (IFE) using *Krt14-creER*. **b**, Percentage of $EPCAM^+$ tumour cells in control and *Fat1*-cKO SCCs. Mean ± s.e.m., two-tailed *t*-test. **c**, Graph showing the distribution of the different $EPCAM^-$ tumour cell subpopulations on the basis of the expression of CD106/VCAM1, CD61/ITGB3 and CD51/ITGAV in *Fat1*-cKO tumours. Mean ± s.e.m. **d**, Haematoxylin and eosin staining, showing representative control and *Fat1*-cKO tumours. Scale bar, 50 µm. **e**, **f**, Immunostaining for GFP, KRT14 or vimentin in representative control (**e**) and *Fat1*-cKO tumour (**f**). Scale bar, 50 µm. **g**, Mouse model of skin SCC allowing the expression of YFP and $Kras^{G12D}$ as well as *p53* and *Fat1* deletion preferentially in the hair follicle lineage using *Lgr5-creER*. **h**, Percentage of $EPCAM^+$ tumour cells in the control and *Fat1*-cKO tumours. Mean ± s.e.m., two-tailed *t*-test. **i**, Graph showing the distribution of the different $EPCAM^-$ tumour cell subpopulations on the basis of the expression of CD106/VCAM1, CD61/ITGB3 and CD51/ITGAV in *Fat1*-cKO tumours. Mean ± s.e.m. **j**, Haematoxylin and eosin staining, showing a representative *Fat1* wild-type and *Fat1*-cKO tumour. Scale bar, 50 µm. **k**, **l**, Immunostaining for KRT14 and vimentin showing the absence of keratin pearls in representative $EPCAM^-$ control SCC (**k**) and the presence of keratin pearls in representative $EPCAM^-$ *Fat1*-cKO SCC (**l**). White arrowheads indicate keratin pearls. Scale bar, 100 µm. **m**, Dot plot showing the number of keratin pearls quantified per field at magnification 20×. $n = 5$ fields quantified per sample, mean ± s.e.m., two-tailed *t*-test. **n**, Mouse model allowing YFP and $Kras^{G12D}$ expression as well as *p53* and *Fat1* deletion in lung epithelial cells using intratracheal instillation of Ad5CMVCre virus. **o**, Immunofluorescence image showing the YFP^+ lung tumours 10 weeks after intratracheal instillation of Ad5CMVCre virus in *Fat1* wild-type and *Fat1*-cKO mice. Scale bar, 1 mm.

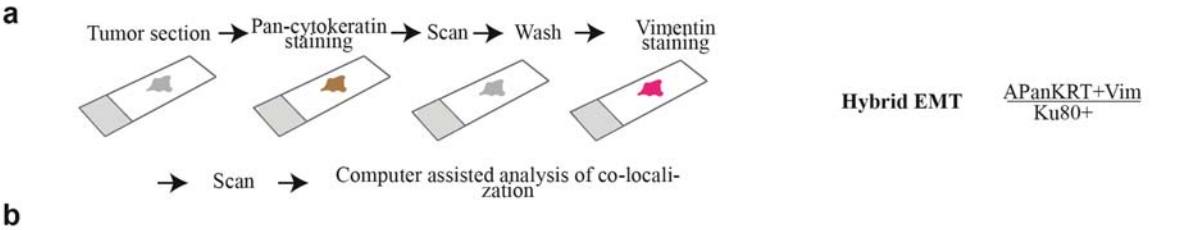

b

Sample ID	Fat1 mutation	Organ origin	Cancer type	Codon	AA change	Exon	Allelic freq	Type of mutation	Prediction (SIFT, Memo PolyPhen)
E48P1	WT	Esophagus	SCC						
E49P2	WT	Esophagus	ADC						
E54P1	WT	Esophagus	SCC						
L75P1	WT	Lung	ADC						
L30P2	WT	Lung	SCC						
L69P2	WT	Lung	SCC						
L6P2	WT	Lung	SCC						
S142P2	WT	Skin	SCC						
HN62P1	WT	Head and Neck	SCC						
L35P2	Mutated	Lung	Pleomorphic carcinoma	p.Thr3284Arg	G -> C	14	0.50	Missense and Splice region variant	Deleterious
P1P3	Mutated	Head and Neck	SCC	p.Arg885*	G -> A	2	0.50	Stop_gained	Deleterious
S159P2	Mutated	Skin	SCC	p.Leu148*	A -> C	2	1.00	Stop_gained	Deleterious
SCS6P2	Mutated	Skin	SCC	p.Thr1585Met	G -> A	9	0.50	Missense	Deleterious
SL14P1	Mutated	Skin	SCC	p.Pro1763Leu	G -> A	10	0.50	Missense	Deleterious
HN6P2	Mutated	Head and Neck	SCC	p.Val3009del	ACT -> X	11	1.00	Disruptive inframe mutation	Deleterious
HN8P2	Mutated	Head and Neck	SCC	p.Tyr372*	G -> T	2	0.50	Stop_gained	Deleterious
L119P2	Mutated	Lung	SCC	p.Gly3179*	C -> A	14	1.00	Stop_gained	Deleterious

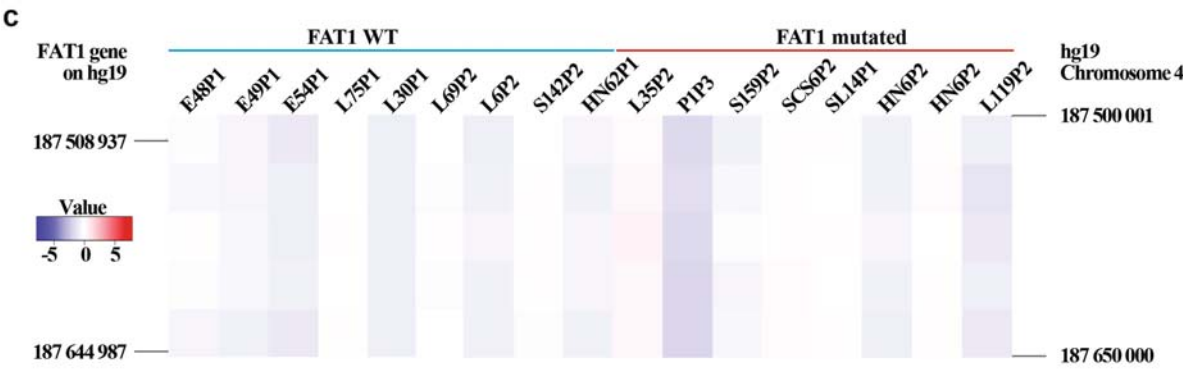

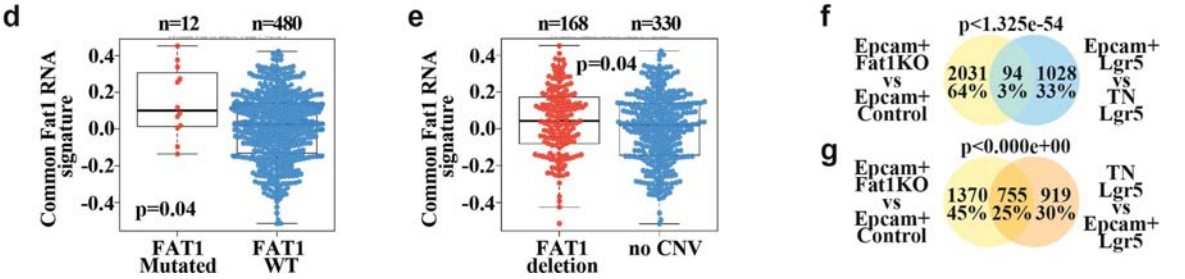

Extended Data Fig. 5 | See next page for caption.

Extended Data Fig. 5 | Mutations in *FAT1* promotes hybrid EMT state in human cancers. a, Schematic representing the method of analysing the co-expression of pan-cytokeratin and vimentin using immunohistochemistry of patient-derived xenografts that present (or not) mutations in *FAT1*, and the definition of hybrid EMT score. **b**, Table summarizing the samples of patient-derived xenografts on which whole-exome sequencing was performed, and detailed information on the mutations: codon, amino acid change, the exon containing the mutation, the allelic frequency, the type of mutations and the bioinformatic prediction of the effect of the mutation on the function of the protein using three bioinformatic algorithms (SIFT, Memo and PolyPhen). **c**, Heat map showing the copy number variation profile of *FAT1* genomic region in the patient-derived xenograft samples included in the analysis of hybrid EMT score. The colour code corresponds to the quantified copy number and the genomic coordinate (reference genome hg19) of bin set for quantification. The *FAT1* gene is marked on each vertical edge. **d**, **e**, Box plot showing the distribution of the common mRNA signature (mouse skin and lung *Fat1*-cKO SCCs and human *FAT1*-knockout SCC cell line) compared to *FAT1* mutation status in human lung SCC (TCGA database; for the analysis, only high-impact mutations in >20% of variant allele frequency were considered) (**d**) and *FAT1* copy number variation status in human lung SCC (TCGA database) (**e**). Boundaries of the box indicate the first and third quartiles of the FAT1 RNA signature value. The bold horizontal line indicates the median and the two external horizontal lines shows the minimum and maximum values. The dots represent all data points. Differences between the two groups are assessed using a two-sided Wilcoxon rank-sum test. **f**, **g**, Venn diagram of the genes upregulated in the EPCAM$^+$ *Fat1*-cKO skin SCC and upregulated in LGR5 EPCAM$^+$ versus triple-negative hybrid EMT tumour cells (**f**) or in triple-negative versus EPCAM$^+$ cells (**g**). Two-sided hypergeometric test.

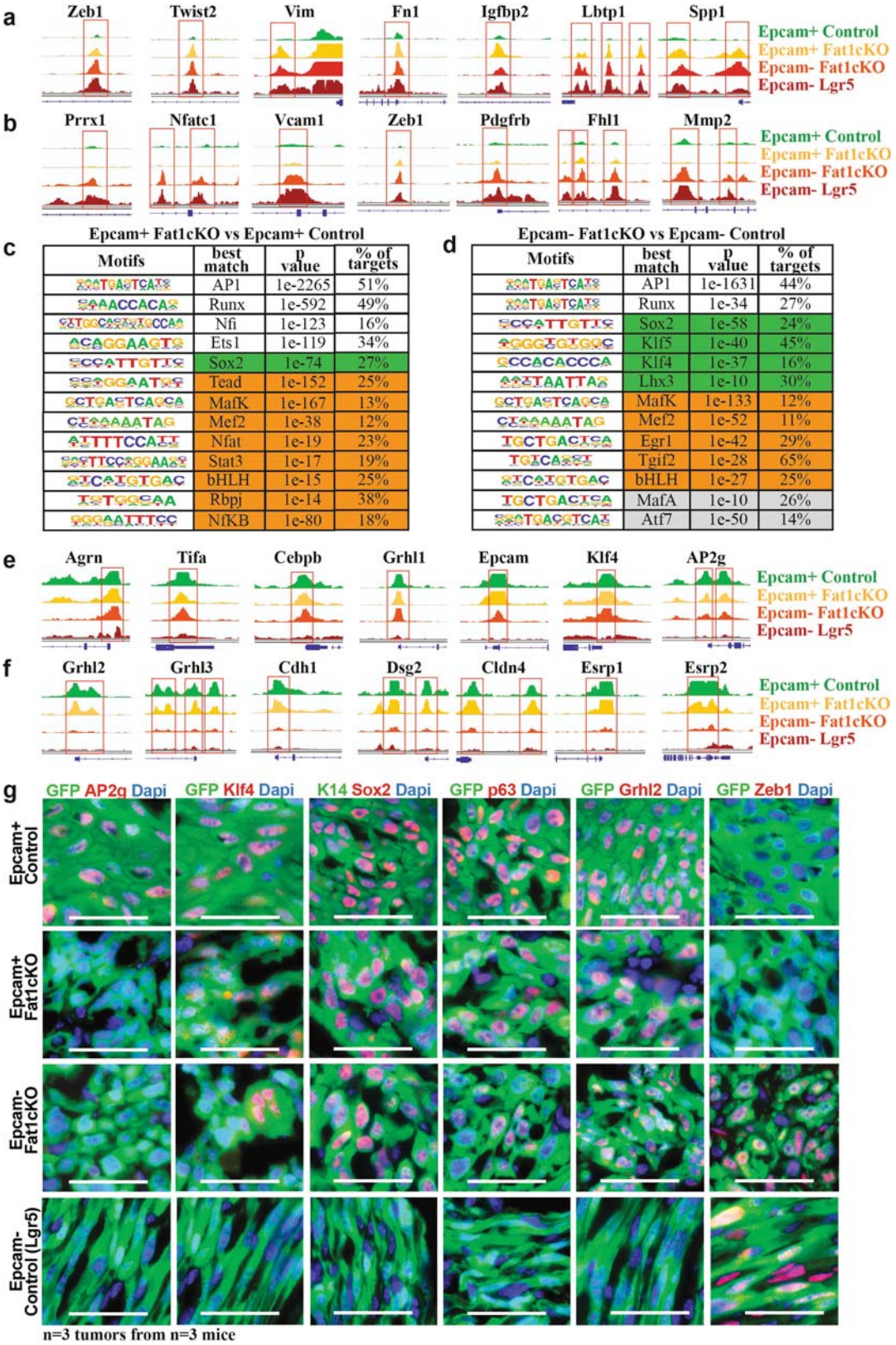

Extended Data Fig. 6 | See next page for caption.

Extended Data Fig. 6 | EPCAM$^+$ *Fat1*-cKO tumour cells are epigenetically primed to undergo EMT, whereas EPCAM$^-$ *Fat1*-cKO sustain the expression of epithelial program. a, ATAC-seq profiles of the chromatin regulatory regions of mesenchymal genes closed in control EPCAM$^+$ tumour cells and opened in EPCAM$^+$ *Fat1*-cKO tumour cells, showing epigenetic priming of EPCAM$^+$ *Fat1*-cKO tumour cells to undergo EMT. **b**, ATAC-seq profiles of the chromatin regulatory regions of mesenchymal genes with open chromatin regions only in EMT EPCAM$^-$ tumour cells. **c**, Transcription factor motifs enriched in the ATAC-seq peaks upregulated between the EPCAM$^+$ *Fat1*-cKO and EPCAM$^+$ control tumour cells as determined by Homer. Cumulative hypergeometric distributions. White boxes show core transcription factors; boxes highlighted in green show epithelial transcription factors; and boxes highlighted in orange show EMT transcription factors. **d**, Transcription factor motifs enriched in the ATAC-seq peaks that are upregulated between the EPCAM$^-$ *Fat1*-cKO and EPCAM$^-$ control tumour cells as determined by Homer analysis. Cumulative hypergeometric distributions. White boxes show core transcription factors; boxes highlighted in green show epithelial transcription factors; boxes highlighted in orange show EMT transcription factors; and boxes highlighted in grey show other transcription factors. **e**, ATAC-seq of the chromatin regulatory regions of epithelial genes with open chromatin regions in EPCAM$^-$ *Fat1*-cKO tumour cells as compared to EPCAM$^-$ tumour cells from LGR5-derived SCCs, showing the sustained opening of epithelial enhancers in EPCAM$^-$ *Fat1*-cKO tumour cells. **f**, ATAC-seq of the chromatin regulatory regions of epithelial genes that are closed upon EMT, irrespective of *Fat1* deletion. **g**, Immunostaining for GFP and AP2G, KLF4, SOX2, p63, GRHL2 or ZEB1 in EPCAM$^+$ and EPCAM$^-$ control and *Fat1*-cKO DMBA/TPA skin SCCs. Scale bar, 50 µm.

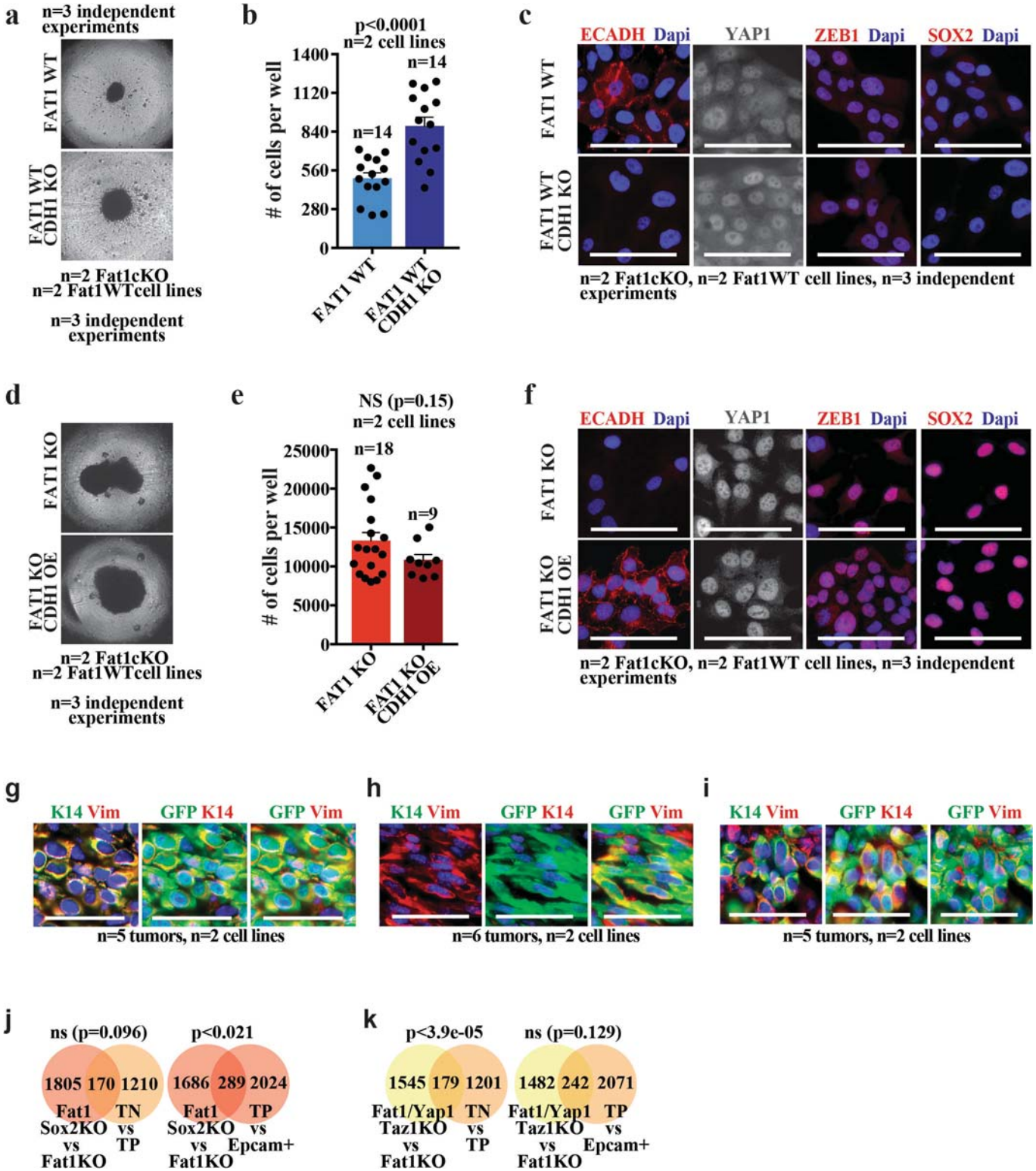

Extended Data Fig. 7 | Loss of cell adhesion is not sufficient to induce the hybrid EMT phenotype. a, Images showing spheroids formed 7 d after plating 4,000 *FAT1* wild-type or *FAT1* wild-type, *CDH1*-knockout human A388 skin SCC cells on an ultra-low adherent plate. **b**, Bar chart showing the quantification by FACS of the number of cells in *FAT1* wild-type, and *FAT1* wild-type and *CDH1*-knockout, spheroids. Mean + s.e.m., two-tailed *t*-test. **c**, Immunostaining for E-cadherin, YAP1, ZEB1 and SOX2 in *FAT1* wild-type, and *FAT1* wild-type and *CDH1*-knockout, tumour cells. Scale bar, 50 µm. **d**, Images showing spheroids formed 7 d after plating 4,000 *FAT1*-knockout or *FAT1*-knockout and *CDH1*-overexpressing human A388 skin SCC cells on an ultra-low attachment plate. **e**, Bar chart showing the quantification by FACS of the number of cells in *FAT1*-knockout or *FAT1*-knockout and *CDH1*-overexpressing spheroids. Mean + s.e.m., two-tailed *t*-test. **f**, Immunostaining for E-cadherin, YAP1, ZEB1 and SOX2 in *FAT1*-knockout or *FAT1*-knockout and *CDH1*-overexpressing tumour cells. Scale bar, 50 µm. **g**–**i**, Immunostaining of K14 and vimentin after subcutaneous transplantation of *Fat1*-cKO (**g**), *Fat1* and *Sox2* double-knockout (**h**) or *Fat1*, *Yap1* and *Taz* triple-knockout (**i**) mouse skin SCC cells. Mean ± s.e.m. Scale bars, 50 µm. **j**, **k**, Venn diagram of the genes upregulated in EPCAM$^-$ *Fat1*-cKO skin SCC upon *Sox2* deletion (**j**) or upon *Yap1* and *Taz* deletion (**k**), and upregulated genes in hybrid EMT triple-negative cells versus late EMT triple-positive cells (early hybrid EMT signature) and in triple-positive versus EPCAM$^+$ cells (late EMT signature). Two-sided hypergeometric test.

a Kinases phosphorylated in FAT1 WT

Kinase	FC (WT/KO)	p value
AKT2	7.7	0.0260
MAP4K4	6.6	0.0232
PRKCD	6.6	1.25E-05
ERBB2	5.9	0.0035
CLK2	5.9	0.0047
STK10	5.6	0.0034
MAP2K1 (MEK1)	5.3	0.0413
EGFR	5.3	0.0094
PTK2B	4.8	0.0002
MAP2K2 (MEK2)	4.5	0.0353
MAP2K6/MAP2K3	4.5	0.0534
MTOR	4.2	0.0009
STK3	4.2	0.0003
ZAK	4.0	0.0047
PAK6/PAK7	3.9	0.0125
PRPF4B	3.6	0.0075
PRKD3	3.3	0.0026

b

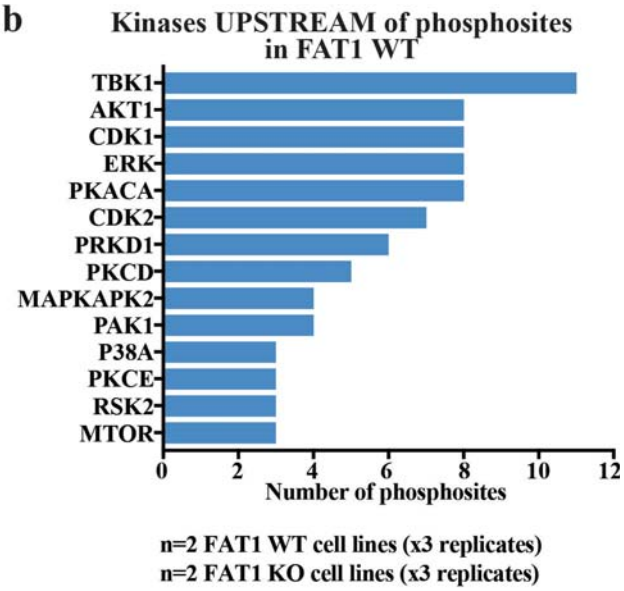

c Kinases phosphorylated in FAT1cKO

Kinase	FC (KO/WT)	p value
YES1	10.8	3.97E-09
CDK11	9.9	0.0087
PRPF4B	8.1	0.0121
BMP2K	5.0	0.0090
CDK12	4.2	2.96E-05
PNKP	3.6	0.0004
MNAT	3.3	9.83E-07
MINK	3.0	0.0001

d

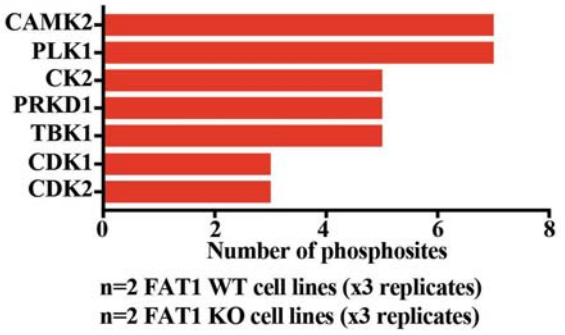

e

Kinase	Phosphosites	
CAMK2	CD44_S706	GJA1_S330
	GJA1_S325	GJA1_S364
	GJA1_S328	GJA1_S365
	GJA1_S306	

f

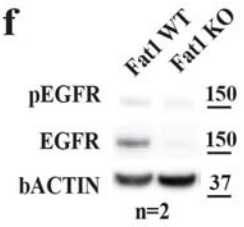

g

h

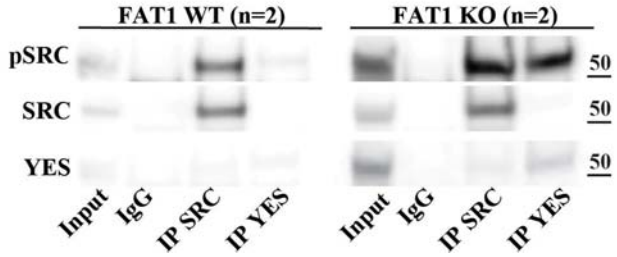

Extended Data Fig. 8 | See next page for caption.

Extended Data Fig. 8 | Phosphoproteomic analysis reveals signalling cascades downstream of *FAT1* LOF. a, Table showing kinases that are significantly more phosphorylated in *FAT1* wild-type cells as compared to *FAT1*-knockout cells. *t*-test, FDR = 0.05, S_0 = 1. **b**, Bar chart showing the kinases that are predicted to phosphorylate phosphosites significantly enriched in *FAT1* wild-type tumour cells. **c**, Table showing kinases that are significantly more phosphorylated in *FAT1*-knockout cells as compared to *FAT1* wild-type cells. *t*-test, FDR = 0.05, S_0 = 1. **d**, Bar chart showing the kinases that are predicted to phosphorylate phosphosites that are significantly enriched in *FAT1*-knockout tumour cells. **e**, Table showing the sites in *FAT1*-knockout cells predicted to be phosphorylated by CAMK2. **f**, **g**, Western blot showing pEGFR and EGFR (**f**) or pMEK and MEK (**g**) in *Fat1* wild-type and *Fat1*-knockout *Lgr5-creER;Kras^{G12D};p53^{cKO};Fat1$^{fl/fl}$;RYFP* mouse skin SCC cells. **h**, Western blot showing the expression levels of pSRC, total SRC and YES on the input of wild-type and *FAT1*-knockout cells, and upon immunoprecipitation of SRC and YES (n = 4). The apparent molecular weight reference in kDa is indicated close to **f**–**h**.

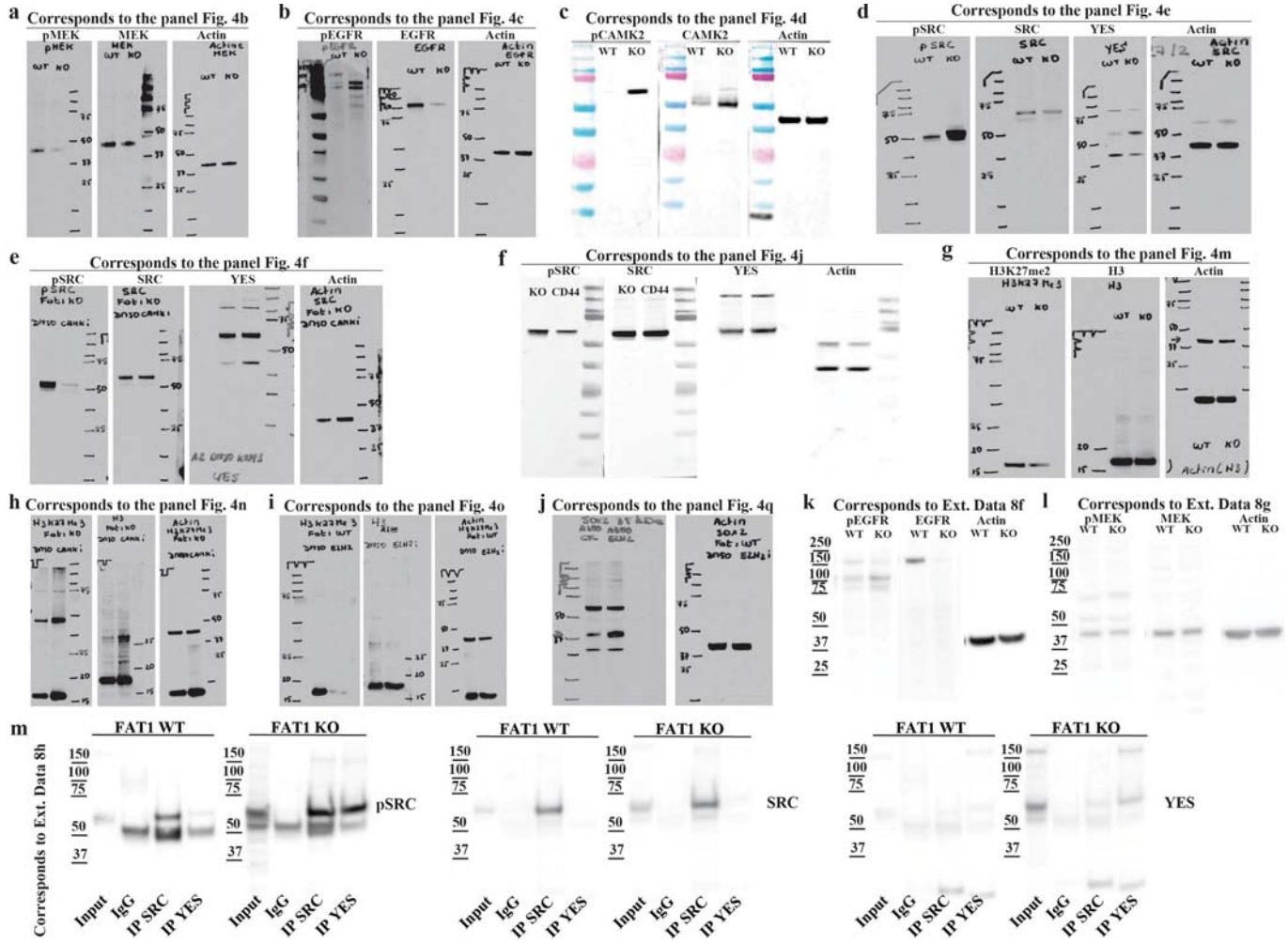

Extended Data Fig. 9 | Full scan of western blot membranes. a–k, Images showing full scan of western blot membranes displayed in Fig. 4. Each panel indicates the figure and the panel to which the full membrane image belongs. Molecular weight size standards are indicated on each membrane. In all the experiments the controls (β-actin) were run on the same gel as the samples.

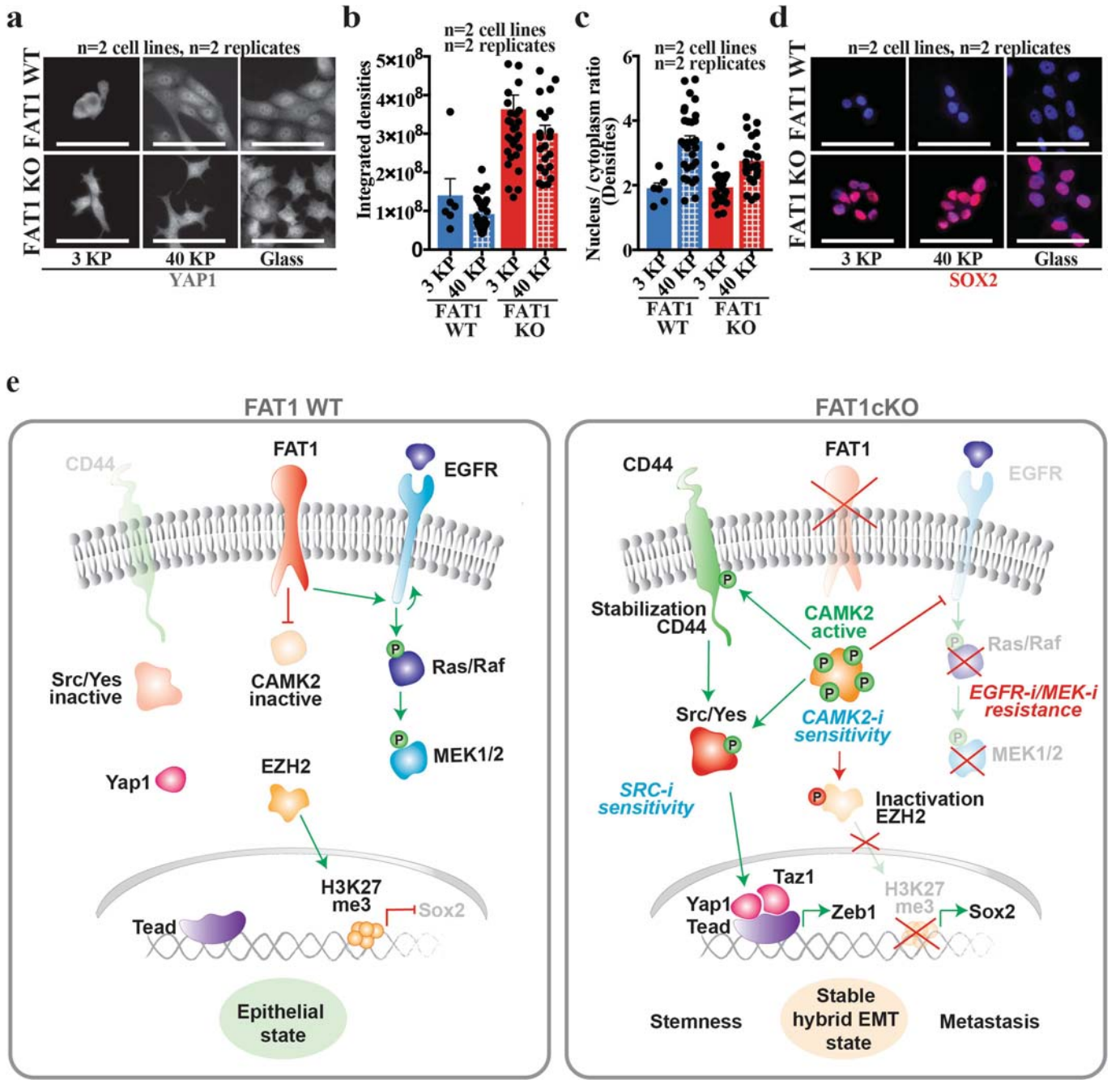

Extended Data Fig. 10 | Increase in YAP1 and SOX2 signalling downstream of *FAT1* LOF is independent of the stiffness of the substrate. a, Immunostaining for YAP1 in *FAT1* wild-type and *FAT1*-knockout human SCC cells upon increasing stiffness conditions. Scale bar, 50 µm. **b**, Quantification of YAP1 expression on the basis of fluorescence intensity in *FAT1* wild-type and *FAT1*-knockout cells in different stiffness conditions. Mean + s.e.m. **c**, Quantification of YAP1 nuclear/cytoplasmic ratio on the basis of fluorescence intensity in *FAT1* wild-type and *FAT1*-knockout cells in different stiffness conditions. Mean + s.e.m. **d**, Immunostaining for SOX2 in *FAT1* wild-type and *FAT1*-knockout human SCC cells in increasing stiffness conditions. Scale bar, 50 µm **e**, Model of the signalling pathways that are activated or repressed in *FAT1*-knockout cells to induce a hybrid EMT state and to predict a differential effect on the response to therapy.

nature research

Corresponding author(s): Cédric Blanpain

☐ Initial submission ☐ Revised version ☒ Final submission

Life Sciences Reporting Summary

Nature Research wishes to improve the reproducibility of the work that we publish. This form is intended for publication with all accepted life science papers and provides structure for consistency and transparency in reporting. Every life science submission will use this form; some list items might not apply to an individual manuscript, but all fields must be completed for clarity.

For further information on the points included in this form, see Reporting Life Sciences Research. For further information on Nature Research policies, including our data availability policy, see Authors & Referees and the Editorial Policy Checklist.

Experimental design

1. Sample size

Describe how sample size was determined.

Samples size for each experiment is indicated in the figures or corresponding figure legends. The sample size was chosen based on previous experience in the lab, for each experiment to yield high power to detect specific effects. The previous experiences refers to: the data on the frequency of appearance of tumors and survival in DMBA/TPA and genetic models of skin SCC, tumor cellular and molecular heterogeneity of the different tumor types, the frequency of metastasis, the frequency of secondary tumors upon subcutaneous transplantation and the heterogeneity of the secondary tumors, tumor propagating cell frequency, etc (Pastushenko Nature 2018, Latil Cell Stem Cell 2017, Beck Cell Stem Cell 2015, Boumahdi Nature 2014, Revenco Cell Rep 2019, Lapouge EMBO J 2012). No statistical methods were used to predetermine sample size.

2. Data exclusions

Describe any data exclusions.

No data were excluded from the analysis

3. Replication

Describe whether the experimental findings were reliably reproduced.

All the experiments were performed in at least 3 biologically independent replicates. All replicates reported in the manuscript and on which statistics are based are biological replicates. No technical replicates were used to calculate statistics. All attempts at replication of the results were successful.

4. Randomization

Describe how samples/organisms/participants were allocated into experimental groups.

For in vivo studies on primary mouse models, animals were chosen based on correct genotypes: requiring 2 (K14Cre/RYFP, Fat1/RYFP, K14CreER/Fat1), 3 (K14Cre/Fat1/RYFP), 4 (Lgr5CreER/Kras/p53/RYFP, K14CreER/Kras/p53/RYFP and Kras/p53/Fat1/RYFP) or 5 correct alleles (Lgr5CreER/Kras/p53/Fat1/RYFP or K14CreER/Kras/p53/Fat1/RYFP).
K14Cre and K14CreER mice were treated with DMBA/TPA at the age of 6-8 weeks after virth and the mice developed tumors in 4-10 months. K14CreER/Kras/p53 mice were induced with Tamoxifen at a age 28-35 days after birth, and the mice developed tumours in 2-3 months, thus minimizing the difference in age of different animals used. Kras/p53/Fat1/RYFP mice were treated with intratracheal instillation of AdeCRE virus at the age of 6-12 weeks.
Sex-specific differences were minimized by including similar numbers of male and female animals. Each experiment contained animals from at least 3 different litters. In the subcutaneous or intravenous grafting experiments we used NOD/Scid/Il2 mice of similar age and both female and male.
For experiments involving cell culture no allocation in groups was needed. For the drug screening in vitro both FAT1 WT and FAT1 KO cells were treated with all the drugs, so no allocation in groups or randomization was required.

5. Blinding

Describe whether the investigators were blinded to group allocation during data collection and/or analysis.

Investigators were blinded to mouse genotypes during experiments, for performing sample analysis, imaging and quantification.
For experiments with cell lines the researchers were blinded to cell line genotypes or treatment conditions for analysis, imaging and quantification.

Note: all studies involving animals and/or human research participants must disclose whether blinding and randomization were used.

6. Statistical parameters

For all figures and tables that use statistical methods, confirm that the following items are present in relevant figure legends (or in the Methods section if additional space is needed).

n/a	Confirmed	
☐	☒	The exact sample size (*n*) for each experimental group/condition, given as a discrete number and unit of measurement (animals, litters, cultures, etc.)
☐	☒	A description of how samples were collected, noting whether measurements were taken from distinct samples or whether the same sample was measured repeatedly
☐	☒	A statement indicating how many times each experiment was replicated
☐	☒	The statistical test(s) used and whether they are one- or two-sided (note: only common tests should be described solely by name; more complex techniques should be described in the Methods section)
☒	☐	A description of any assumptions or corrections, such as an adjustment for multiple comparisons
☐	☒	The test results (e.g. *P* values) given as exact values whenever possible and with confidence intervals noted
☐	☒	A clear description of statistics including central tendency (e.g. median, mean) and variation (e.g. standard deviation, interquartile range)
☐	☒	Clearly defined error bars

See the web collection on statistics for biologists for further resources and guidance.

Software

Policy information about availability of computer code

7. Software

Describe the software used to analyze the data in this study.

The Chi square and t-test were performed using Prism (version 8). The RNA-sequencing data were analyzed using STAR software (2.4.2a). Peak calling was performed by macs (version 2.1.0.20151222). Peaks were associated to genes with GREAT software (4.0.4). The data were analyzed using R software (3.2.3).
Exome sequencing analysis: bedtools (Version 2.27.0) and ANNOVAR (v2013Jun21).
Flow cytometry: FACS ARIA III (for FACS sorting) and FACSDiva software (for FACS data analysis).

For manuscripts utilizing custom algorithms or software that are central to the paper but not yet described in the published literature, software must be made available to editors and reviewers upon request. We strongly encourage code deposition in a community repository (e.g. GitHub). *Nature Methods* guidance for providing algorithms and software for publication provides further information on this topic.

Materials and reagents

Policy information about availability of materials

8. Materials availability

Indicate whether there are restrictions on availability of unique materials or if these materials are only available for distribution by a for-profit company.

Raw data from RNA-seq, ATAC-seq, Whole Exome Sequencing and low coverage Whole Genome Sequencing have been deposited to a public database under the following codes: GSE158502 (mouse RNA-seq), GSE158501 (human RNA-seq), GSE158500 (ATACseq), GSE158503 (WES) and GSE158505 (low-cogerave WGS) . All materials are readily available from the authors or from standard commercial sources. There are no restrictions on availability of the materials used in the study.

9. Antibodies

Describe the antibodies used and how they were validated for use in the system under study (i.e. assay and species).

For FACS analysis and sorting the following antibodies were used:
CD51 (rat clone RMV-7, Biolegend Cat#104106, dilution 1:50), BV421-conjugated anti-CD61 (Armenian hamster, clone 2C9.G2, BD Bioscience Cat#553345, dilution 1:50), biotin-conjugated anti-CD106 (rat, clone 429 (MVCAM.A), BD Bioscience Cat#553331, dilution 1:50), BV711-conjugated anti-Epcam (rat clone G8.8, BD Bioscience Cat#563134, dilution 1:100), PerCPCy5.5 conjugated anti-CD45 (rat, clone 30-F11, BD Bioscience Cat#550994, dilution 1:100) and PerCPCy5.5 conjugated anti-CD31 (rat, clone MEC 13.3, BD Bioscience Cat#562861, dilution 1:100), APC conjugated anti-CD44 (rat, clone IM7, Biolegend, Cat#103011, 1:100)

For Immunofluorescence and Immunohistochemistry the following antibodies were used:
Primary antibodies: Anti-GFP (goat polyclonal, Abcam Cat#ab6673, 1:400), anti-K14 (chicken polyclonal, Thermo Fisher Scientific Cat#MA5-11599, 1:1000), anti-K10 (rabbit, polyclonal, Covance/IMITEC Cat#PRB-159P-0100, 1:1000), anti-Krt5 (rabbit polyclonal, BioLegend Cat#905501/Formerly Covance Antibody Product Cat# PRB-160P, 1:1000), Anti-Krt7 (Rabbit monoclonal antibody, clone EPR1619Y, Abcam Ct#ab68459, 1:200), anti-Itgb4 (rat, clone 346-11A, BD Cat#553745, 1:200), anti-Vimentin (rabbit, clone ERP3776, Abcam Cat#ab92547, 1:500), anti-E-Cadherin (rat, clone ECCD-2, Invitrogen Cat#13-1900, 1:200), anti-YAP1 (for IF rabbit, polyclonal, Proteintech Cat#13584-1-AP; for IHC rabbit, polyclonal, SantaCruz Cat#sc-15407, 1:50), anti-Sox2 (rabbit, clone ERP3131, Abcam Cat#ab92494, 1:200), anti-Grhl2 (rabbit, polyclonal, Sigma, Cat#HPA004820, 1:50), Anti-Klf4 (rabbit, polyclonal, Abcam Cat#ab129473, 1:50), anti-p63 (rabbit, polyclonal, Abcam Cat#ab97865, 1:50), anti-AP2g (rabbit, polyclonal, Abcam Cat#ab220872, 1:50), anti-Cldn1 (rabbit, polyclonal, ThermoFisher Cat#51-9000, 1:50), anti-Zo1 (mouse, clone ZO1-1A12, ThermoFisher Cat#33-9100, 1:50), anti-Zeb1 (rabbit, polyclonal Bethyl/IMITEC Cat#IHC-00419, 1:200), anti-CD44-APC (rat, clone IM7, Biolegend, Cat#103011, 1:50)
The following secondary antibodies were used: anti-rabbit, anti-rat, anti-goat, anti-chicken, anti-mouse conjugated to rhodamine Red-X (Jackson ImmunoResearch - Cat.#711-295-152; 712-295-153; 705-295-147; 703-295-155; 715-295-151), Alexa Fluor 647 (Jakson ImmunoResearch - Cat.#711-605-152; 712-605-153 ; 705-605-147; 703-605-155; 715-605-150) or to Alexa Fluor-A488 (Molecular Probes - Cat.#A21206; A21208; A11055; A11039; A21202).
For immunohistochemistry the VECTASTAIN ABC-HRP Kit, Peroxidase (Rabbit IgG) - (PK-4001) has been used (Vector Laboratories).

For Western Blot the following antibodies were used:
Anti-phospho-CAMK2 (Rabbit, 1/133, Cell Signaling, clone D21E4, cat#12716), anti-phospho-SCR Tyr416 (Rabbit, 1:3000, Cell Signaling, clone D49G4, Cat#6943), anti-H3K27Me3 Lys27 (Rabbit, 1:3000, Millipore, Cat#17-622), anti-phospho-MEK1/MEK2 Ser218, SER222, Ser226 (Rabbit, 1:1000, Invitrogen, Cat#44-454G), anti-phospho-EGFR Y1197 (Rat, 1:500, R&D, MAB8058), anti–CAMK2 (pan) (Rabbit, 1/125, Cell Signaling, clone D11A10, cat#4436), anti-SRC (Rabbit, 1:1000, Cell Signaling, clone32G6, Cat#2123) or anti-H3 (Rabbit, 1:6000, Abcam, Cat#ab1791), anti–MEK1/MEK2 (Rabbit, 1:1000, Invitrogen, Cat#PA5-31917), anti-EGFR (Rabbit, 1:1000, Cell Signaling, clone D38B1, Cat#4267), anti-YES (Rabbit, 1:1000, Cell Signaling, clone D9P3E, Cat#65890) and anti–β-actin (1:2000, Abcam, Cat#ab8227). Anti-rabbit or anti-rat immunoglobulin G (IgG) conjugated with horseradish peroxidase (HRP) (1:3000 or 1:5000; Healthcare) was used as the secondary antibody. The antibodies are commercially available and were validated by the provider. We used the protocols and recommendations of the manufacturer only on validated species (mouse or human).

For ChIP rabbit monoclonal antibody for H3K27me3 (C36B11 Rabbit mAb, #9733 Cell Signaling Technologies) was used.

10. Eukaryotic cell lines

a. State the source of each eukaryotic cell line used.

A388 (human skin SCC cell), primary mouse skin SCC cell lines (derived from Lgr5/Kras/p53 Fat1 WT and Fat1cKO skin SCC).

b. Describe the method of cell line authentication used.

None of the cell lines have been authenticated.

c. Report whether the cell lines were tested for mycoplasma contamination.

The cell lines were not tested for mycoplasma contamination.

d. If any of the cell lines used are listed in the database of commonly misidentified cell lines maintained by ICLAC, provide a scientific rationale for their use.

None of the cell lines used are listed in the database of commonly misidentified cell lines maintained by ICLAC.

Animals and human research participants

Policy information about studies involving animals; when reporting animal research, follow the ARRIVE guidelines

11. Description of research animals

Provide details on animals and/or animal-derived materials used in the study.

All the animals used were grown in mixed background.
K14Cre/RYFP, Fat1/RYFP, K14CreER/Fat1, K14Cre/Fat1/RYFP were treated 3 times with DMBA 6-8 weeks after birth and after received treatment with TPA twice a week until the tumors appeared.
Lgr5CreER/Kras/p53/RYFP, K14CreER/Kras/p53/RYFP, Lgr5CreER/Kras/p53/Fat1/RYFP and K14CreER/Kras/p53/Fat1/RYFP mice were induced with Tamoxifen at 28-35 days after birth.
The mice were sacrificed if tumour reached the size allowed by ethical protocol or if mice presented signs of distress or weight loss >20% was observed. The average weight of the mice used was 35g (range from 22 to 48g).
For grafting experiments NOD/SCID/Il2Rγ mice were used with age ranging from 4 to 8 weeks. Both male and female mice were used for these experiments. The weight of these mice was in average 29 g (ranging from 21 to 37g).
For qPCR, ATAC-qPCR, RNA-sequencing, ATAC-sequencing and grafting experiments (subcutaneous and intravenous grafting into immunodeficient mice) subpopulations of cancer cells isolated from primary tumors were used. Sections of prefixed frozen or paraffin embedded primary tumors, organs or skin were used for immunostaining.
NOD/SCID/Il2Rγ null mice were used for transplantation and metastasis assays (by performing subcutaneous and intravenous grafting of tumor cells)
For lung cancer experiments Kras/p53/RYFP and Kras/p53/RYFP/Fat1KO mice were treated with intratracheal instillation of AdenoCre. The mice were followed up daily and were sacrificed if any signs of respiratory distress, weight loss or deterioration of general condition were detected.
The housing conditions of all animals were strictly following the ethical regulations. The room temperature ranged from 20 and 25°C. The relative ambient humidity at the level of mouse cages was 55 per cent +/-15. Each cage was provided with food, water and two types of nesting material. Semi-natural light cycle of 12:12 was used.

Policy information about studies involving human research participants

12. Description of human research participants

Describe the covariate-relevant population characteristics of the human research participants.

Samples of human cancers were included. All the cases for which the Whole Exome Sequencing data (that allow identification of FAT1 mutation) were available were included in the study. All the patients included in the Patient Derived Xenograft platform gave their consent and the study was approved by the all relevant institutions. The researchers involved in this work did not have access to the clinical data (such as age or gender). All the samples received were asigned by the clinican or surgeon responsible for patient care a unique code.

nature research

Corresponding author(s): Cédric Blanpain

☐ Initial submission ☐ Revised version ☒ Final submission

Flow Cytometry Reporting Summary

Form fields will expand as needed. Please do not leave fields blank.

Data presentation

For all flow cytometry data, confirm that:

☒ 1. The axis labels state the marker and fluorochrome used (e.g. CD4-FITC).

☒ 2. The axis scales are clearly visible. Include numbers along axes only for bottom left plot of group (a 'group' is an analysis of identical markers).

☒ 3. All plots are contour plots with outliers or pseudocolor plots.

☐ 4. A numerical value for number of cells or percentage (with statistics) is provided.

Methodological details

5. Describe the sample preparation.	Skin tumors from DMBA/TPA treated mice, Lgr5CreER/Kras/p53/Fat1cKO/RYFP and K14CreER/Kras/p53/Fat1cKO/RYFP or lung tumors from Kras/p53/Fat1cKO/RYFP mice were dissected, minced and digested in Collagenase type I (Sigma) at 3.5 mg/ml during 1 hour at 37ºC on a rocking plate protected from light. Collagenase activity was blocked with by the addition of EDTA (5mM) and then the cells were rinsed in PBS supplemented with 2% FBS and the cell suspensions were filtered through a 70um cell strainers (BD).
6. Identify the instrument used for data collection.	FACSAria and LSRFortessa (BD Bioscience)
7. Describe the software used to collect and analyze the flow cytometry data.	FACSDiva and FACSAria Software (BD Bioscience)
8. Describe the abundance of the relevant cell populations within post-sort fractions.	The proportion of YFP+ tumor cells in Lin- population varied from 20 to 95%. The proportion of tumor cell subpopulations within YFP+ tumor cells varied depending on the tumor type and between individual tumors.
9. Describe the gating strategy used.	Living cells were selected by forward scatter, side scatter, doublets discrimination and by 7AAD dye exclusion. Tumor cell subpopulations were selected based on the expression of YFP and the exclusion of CD45 and CD31.

Tick this box to confirm that a figure exemplifying the gating strategy is provided in the Supplementary Information. ☒